RADIATION SHIELDING PROPERTIES OF FEW NATURAL ROCKS

A Dissertation

Submitted to the 'Dean Office, Institute of Science & Technology'
in the Partial Fulfillment for the Requirement of Master's Degree of Science in Physics

By

Uddab Bahadur Bhandari

Exam Roll No.: PHY 3611/076

T.U. Regd. No.: 5-2-0061-0185-2015

November 12, 2024

Recommendation

It is certified that **Mr. Uddab Bahadur Bhandari** has carried out the dissertation entitled "**RADIATION SHIELDING PROPERTIES OF FEW NATURAL ROCKS**" under our supervision. We recommend the dissertation in the partial fulfillment of the requirement of Master's Degree of Science in Physics.

.....

(Supervisor)
Dr. Raju Khanal
Professor
Central Department of Physics
Tribhuvan University
Kathmandu, Nepal

.....

(Co-Supervisor)
Mr. Devendra Raj Upadhyay
Lecturer
Department of Physics, Amrit Campus
Tribhuvan University
Kathmandu, Nepal

Acknowledgements

Foremost, I would like to express my deep gratitude and sincere respect to my Supervisor Prof. Dr. Raju Khanal, Central Department of Physics, Tribhuvan University and Co-Supervisor Mr. Devendra Raj Upadhyay, lecturer of physics, Amrit Campus, Tribhuvan University for their continuous support to my work. His constant guidance helped me to complete my research work in proper time. Without their scientific vision, understanding of the subject and tactfulness to deal with student, the dissertation would have never taken this present form. I am thankful to the Head of Department of Physics, Amrit Campus, Thamel, Kathmandu Assoc. Prof. Dr. Janak Ratna Malla also gratitude towards M.Sc. physics coordinator of Amrit Campus Asst. Prof. Pitamber Shrestha also Prof. Dr. Rajendra Parajuli, Prof. Dr. Leela Pradhan Joshi (Immediate past Head of Department) and all other my respected professor. I would like to acknowledge the support from International Atomic Energy Agency (IAEA) for establishing the Nuclear Research Laboratory at Central Department of Physics, Tribhuvan University, Kirtipur (through TC project NEP0002) and Ministry of Education, Science and Technology, Government of Nepal (for coordination with IAEA). I am grateful to the Province Government, Ministry of Industry, Tourism, Forest and Environment, Sudurpaschim province for financial support. I would also like to thanks to my friends at Amrit Campus for making the last two years one of the most memorable and enriching time of my life, especially Mr. Birendra Khadka who always took the time to discuss questions about my research and whose insights were really helpful to my dissertation work.

Finally, my family have been a great source of strength and motivation for me all throughout, I dedicate this dissertation work to them for their unconditional love and support. Without their support, it is difficult for me to complete my dissertation.

Evaluation

We certify that we have read this dissertation work entitled "**RADIATION SHIELDING PROPERTIES OF FEW NATURAL ROCKS**". In our opinion, it qualifies in the scope and quality as dissertation in partial fulfillment for the requirement of Master's Degree of Science in Physics.

Evaluation Committee

.....

(Supervisor)
Dr. Raju Khanal
Professor
Central Department of Physics
Tribhuvan University

.....

(Co-Supervisor)
Mr. Devendra Raj Upadhyay
Lecturer
Department of Physics
Amrit Campus
Tribhuvan University

.....

Assoc. Prof. Dr. Janak Ratna Malla
Head of Department
Department of Physics
Amrit Campus
Tribhuvan University
Kathmandu, Nepal

.....

Asst. Prof. Pitamber Shrestha
M.Sc. Coordinator
Department of Physics
Amrit Campus
Tribhuvan University
Kathmandu, Nepal

.....

Internal

.....

External

Sep. 6, 2024

Abstract

Radiation shielding is the practice of protecting people and the environment from the harmful effect of ionizing radiation. The chemical composition of the five rock sample named as Quartz-I, Phyllite, Granite, Quartz-II and Sandstone is determined by Inductively Coupled Plasma Optical Emission Spectroscopy (ICP OES). Radiation shielding properties of rock samples is analyzed by using the Phy-X/PSD software within the energy range 15 keV to 15 MeV. We measure the various parameters such as linear attenuation coefficient (*LAC*), mass attenuation coefficient (*MAC*), half value layer (*HVL*), tenth value layer (*TVL*), mean free path (*MFP*), fast neutron removal cross-section (*FNRCS*), effective atomic number (Z_{eff}) and efficient conductivity (C_{eff}). High mass attenuation coefficient (*MAC*) values is obtained as 6.54 $\text{cm}^2\ \text{g}^{-1}$ for phyllite and low *MAC* values is obtained as 5.08 $\text{cm}^2\ \text{g}^{-1}$ for Quartz-II rock. Similarly phyllite has highest linear attenuation coefficient (*LAC*) value as 17.46 cm^{-1} and sandstone has lowest *LAC* value as 13.42 cm^{-1}. The highest half value layer *HVL* is found to be 3.75 cm for sandstone rock and the lowest *HVL* value is 3.08 cm for Phyllite rock. The highest tenth value layer *TVL* is found to be 12.47 cm for sandstone rock and the lowest *TVL* value is 10.22 cm for Phyllite rock. The effective atomic number (Z_{eff}) was found to be maximum as 15.09 for Phyllite and minimum as 14.04 for Granite. Sandstone has highest mean free path (*MFP*) value found as 5.42 cm and Phyllite has lowest *MFP* value found as 4.44 cm. Phyllite rock has smaller the value of *HVL*, *TVL* and *MFP* so more will be the photon attenuation capacity. The effective atomic number Z_{eff} was found to be maximum as 15.09 for Phyllite and minimum for 14.04 for Granite. Whole obtained data depicts that among the studied rock sample, Phyllite sample is best for shielding purposes among five samples and Sandstone has least shielding ability among selected five rock sample.

Keywords:

Radiation shielding, ICP-OES, Phy-X/PSD software, Attenuation coefficient

शोधसार

विकिरण प्रतिरोध भनेको आयनाइजिङ विकिरणको हानिकारक प्रभावबाट मानिसहरू र वातावरणलाई सुरक्षित राख्ने प्रक्रिया हो। रेडियोधर्मी पदार्थहरूको सुरक्षित भण्डारण, त्यसको निरिक्षण र प्रयोगपछि सुरक्षित रूपमा निराकरण गर्न नेपालका चट्टानहरु प्रयोग गर्न सकिन्छ कि भनेर नेपालका विभिन्न ठाउँबाट क्वार्ट्ज–I, फाइलाइट, ग्रेनाइट, क्वार्ट्ज–II र सेन्डस्टोन नामक पाँचवटा चट्टानका नमूनाहरूको विकिरण प्रतिरोध गर्नसक्ने गुणहरू PhyX/PSD को प्रयोग गरेर विश्लेषण गरियो । PhyX/PSD सफ्टवेयरको ऊर्जा शक्ति १५ keV देखि १५ MeV थियो। ICP–OES द्वारा चट्टानहरुको रसायनिक तत्वको रचना थाहा पाइयो। चट्टानमा भयका तत्व हरुलाई PhyX/PSD सफ्टवेयरको प्रयोग गरि रेखिय विकिरण रोक्ने गुणांक LAC, पिण्डले विकिरण रोक्ने गुणांक MAC, विकिरणको शक्ति आधा पार्ने तह HVL, विकिरणको शक्ति नब्बे प्रतिशतले घटाउने तह TVL, वस्तुको प्रभावकारि परमाणु संख्या Z_{eff}, वस्तुको प्रभावकारी चालकता C_{eff}, वस्तुको प्रभावकारी ईलेक्ट्रोन घनत्व N_{eff}, द्रुत न्यूट्रॉनको टक्कर हुने सम्भावना $FNRCS$ को विश्लेषण गरियो। जसबाट फाइलाइट चट्टानको उच्चतम प्रतिरोधक गुण र सेन्डस्टोन चट्टानको कम प्रतिरोधक गुण भयको पाइयो। फाइलाइट चट्टानको उच्चतम MAC मान ६.५४ से.मि. प्रति ग्राम र फाइलाइट चट्टानको न्युनतम MAC मान ५.०८ से.मि. प्रति ग्राम प्राप्त गरियो। त्यसैगरी LAC को उच्चतम मान फाइलाइट चट्टानमा १७.४६ प्रति से.मि. र न्युनतम मान सेन्डस्टोन चट्टानमा १३.४२ प्रति से.मि. प्राप्त गरियो । HVL को उच्चतम मान सेन्डस्टोन चट्टानमा ३.७५ से.मि. र न्युनतम मान फाइलाइट चट्टानमा ३.०८ से.मि. प्राप्त गरियो । Z_{eff} को उच्चतम मान फाइलाइट चट्टानमा १५.०९ र न्युनतम मान सेन्डस्टोन चट्टानमा १४.०४ प्राप्त गरियो । त्यसैगरी TVL को उच्चतम मान सेन्डस्टोन चट्टानमा १२.४७ से.मि. र न्युनतम मान फाइलाइट चट्टानमा १०.२२ से.मि. प्राप्त गरियो । MFP को उच्चतम मान सेन्डस्टोन चट्टानमा ५.४२ से.मि. र न्युनतम मान फाइलाइट चट्टानमा ४.४४ से.मि. प्राप्त गरियो। Z_{eff}, C_{eff}, N_{eff} र $FNRCS$ को उच्चतम मान फाइलाइट चट्टानमा र न्युनतम मान सेन्डस्टोन चट्टानमा प्राप्त गरियो । सम्पूर्ण प्राप्त तथ्याङ्कको विश्लेसण गर्दा अध्ययन गरिएका पाँचवटा चट्टानहरुमध्ये फाइलाइट चट्टानको विकिरण प्रतिरोध गुण सबैभन्दा उत्तम पाइयो भने सेन्डस्टोन को विकिरण प्रतिरोध गर्ने क्षमता कम भएको पाइयो।

List of Figures

List of Tables

Acronyms and Abbreviations

ACS Atomic Cross Section.

C_{eff} Effective Conductivity.

N_{eff} Effective Electron Density.

Z_{eff} Effective Atomic Number.

ECS Electronic Cross Section.

FNRCS Fast Neutrons Removal Cross Section.

LAC Linear Attenuation Coefficient.

MAC Mass Attenuation Coefficient.

MFP Mean Free Path.

RPE Radiation Protection Efficiency.

TVL Tenth Value Layer.

Fe Iron.

ICP-OES Inductively Coupled Plasma-Optical Emission Spectrometry.

JAEA Japan Atomic Energy Agency.

KEK High Energy Accelerator Research Organization.

ns Nanosecond.

PHITS Particle and Heavy Ion Transport Code System.

Phy-X/PSD Phy-X/Photon Shielding and Dosimetry.

RF Radio Frequency.

RIST Research Organization for Information Science and Technology.

S m^{-1} siemens per meter.

Si Silicon.

Contents

Chapter 1

Introduction

In a variety of contexts, such as industrial, environmental and medical, effective radiation shielding reduces health risks and improves safety. The 2011 Fukushima nuclear accident and the 1986 Chernobyl radiation leak catastrophe have highlighted the critical necessity for exact and comprehensive research on the durability and efficacy of construction materials used as radiation shields [1]. In Nepal, rocks are used to construct the majority of building. It's critical to investigate how effective rocks are as radiation shields. This was accomplished by taking five rocks samples from five location of Nepal and analyzing them for different radiation shielding characteristics.

1.1 Radiation

Radiation is a type of energy that is emitted as a wave or particles that pass through a medium by a material or source. When radioactive material undergoes radioactive disintegration, it emits various types of radiation with differing intensities and energies. Radiation is simply energy in the form of wave. Generally, there are two types of radiation namely ionizing and non ionizing radiation. High dose ionizing radiations are quite harmful for the living organisms. The spontaneous release of photons and particle radiation from an unstable atomic nucleus is known as radioactivity. In general α, β, and γ are produced from the radioactivity which are ionizing radiations. Radiation is the radiated energy from a source that travels through space and even through matter. It is invisible to human senses and impossible to detect directly. Wilhelm Conrad Roentgen discovered radioactivity (X-Rays) in 1895, and scientists have been exploring and

developing radiation for application in various fields ever since [2]. As a result, radiation is currently applied in a variety of industries, including medical and energy. The use of radiation in many industries has certain negative effects, prompting researchers to investigate for radiation shielding. Natural radiation sources are the most prevalent source of background radiation exposure for the public. The primary source of background radiation is natural radioactivity, which has always exposed individuals to ionizing radiation. Due to the long half-life of the radioactive element contained in the earth's crust, natural radioactivity has existed since the beginning of time [3].
Generally, there are two types of radiation namely ionizing and non ionizing radiation. Ionizing radiation has the ability to displace electrons from the outer orbit of an atom or molecule, resulting in a charged atom or molecule known as an ion.

1.2 Non ionizing radiations

Electromagnetic radiation types that lack sufficient energy to ionize atoms or molecules are referred to as non-ionizing radiation, as they are incapable of releasing tightly bound electrons. This category includes radio waves, microwaves, infrared radiation, visible light, and ultraviolet (UV) radiation (lower end). Non-ionizing radiation is frequently used in communication technology, medical imaging, and everyday home gadgets like microwaves and remote controls. Though typically considered less dangerous than ionizing radiation, excessive exposure to certain forms of radiation, such as ultraviolet (UV) radiation, can nonetheless be harmful to one's health [4].

1.3 Ionizing radiations

Ionizing radiation including nuclear radiation, consists of subatomic particles or electromagnetic waves that have sufficient energy to ionize atoms or molecules by detaching electrons from them [5]. The different types of radiation and their penetration strength against different types of barriers are shown in Figure 1.1 [6]. Ionizing radiation comes in different forms, such as alpha, beta, gamma and neutron ray which are discussing briefly as follows:

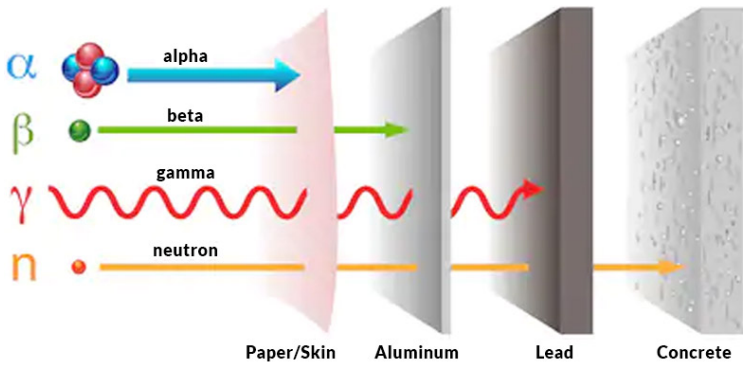

Figure 1.1: Different types of radiation and their penetration strength.

Alpha radiation

Alpha particles, which are helium nuclei made up of two protons and two neutrons, are the source of alpha radiation, a type of ionizing radiation. It is difficult to stop with paper or skin because of its minimal penetrating capacity, but if alpha-emitting materials are swallowed or inhaled, it can be hazardous because to its strong ionizing power. Due to possible health dangers, alpha radiation must be handled carefully even though it is utilized in smoke detectors and targeted cancer therapies. It's a nuclear dissociation reaction in which a radioactive nucleus breaks down and generates alpha particles. Two protons and two neutrons (Z = 2 and A = 4) are emitted by the parent nuclei in this process. The Greek letter alpha denotes a particle that is structurally equivalent to the nucleus of a helium atom and denoted by the Greek letter α. Mathematical representation of Eq. (1.1) shows alpha disintegration process [7].

$$\underset{\text{Parent-isotope}}{{}^{A}_{Z}X} \rightarrow \underset{\text{Alpha-particle}}{{}^{4}_{2}He} + \underset{\text{Daughter-isotope}}{{}^{A-4}_{Z-2}Y} \tag{1.1}$$

Beta radiation

The neutron is changed into a proton and an electron during radioactive disintegration, and the electron is emitted from the atomic nucleus, which is known as the beta particle [8]. The mass of the atom will not change as a result of this operation, but the atomic

number will increase by one. There are two types of beta decays i.e. β^- and β^+
In the case of β^-decay a neutron n transmuted to a proton p with the emission of a β-particle and an anti-neutrino, $\bar{\nu}$. Process can be shown through Eq. (1.2)

$$n \rightarrow p + e^- + \bar{\nu} \tag{1.2}$$

whereas for β^+ decay a proton disintegrates to a neutron with the emission of positron e^+ and neutrino ν. The Eq. (1.3) indicates β^+ decay process.

$$p \rightarrow n + e^- + \nu \tag{1.3}$$

The penetration power of beta radiation is more than alpha particle but less than gamma particle. It can also enter our skin but could not pass through it. So it can be blocked using aluminium sheet or perspex.

Gamma radiation

When radioactive atom nuclei decay, they release high-energy electromagnetic radiation known as gamma radiation. These rays have the potential to cause biological harm because of their high penetration rate and ability to permeate most materials, yet they are also useful in industrial and medicinal situations. Typically, gamma ray shielding uses dense materials, such as concrete or lead, to reduce exposure risks [9].
High-energy photons with shorter wavelengths than X-rays are the defining characteristic of gamma radiation, a kind of electromagnetic radiation. When an atom goes through nuclear processing or radioactive decay, it frequently loses mass. Consequently, the parent atom breaks into two pieces, the nucleus of which always releases extremely sharp gamma rays [10]. Gamma radiation, like X-ray, is electromagnetic radiation that has both a wave and a particle nature, whereas alpha and beta radiation are particles. Protons and neutrons within a nucleus remain constant when a $\gamma-$ ray is released from it, but it has a much greater penetrating power than alpha or beta radiation. It can be blocked with a thick or dense enough covering of high atomic number material. The hottest and most energetic objects in space, such as neutron stars and pulsars, supernova explosions, and

areas around black holes, create them. The decay process is indicated in Eq. (1.4) [11].

$$\underset{\text{Parent-isotope}}{{}^{Am}_{Z}X} \rightarrow \underset{\text{Daughter-isotope}}{{}^{A}_{Z}Y} + \underset{\text{Gamma-particle}}{{}^{0}_{0}\gamma} \tag{1.4}$$

Neutron radiation

Neutron radiation is the product of spontaneous or induced nuclear fission or fusion, which releases free neutrons. Neutron activation, or the ability to convert other materials radioactive, is the most dangerous hazard of neutron radiation. Neutrons have a higher kinetic energy than gamma and beta, making them the most severe and hazardous radiation to the human body when exposed to external radiation sources. It mostly harms soft tissue in the human body, such as the cornea of the eye. Radiation shielding made of hydrogen-rich material can help to reduce the impact of these rays. The disintegration formula is represented in Eq. (1.5) [12].

$$\underset{\text{Parent-isotope}}{{}^{A+B+C}_{Z+Y}X} \rightarrow \underset{\text{Daughter-isotope}}{{}^{A}_{Z}X + {}^{B}_{Y}X} + \underset{\text{neutrons}}{{}^{1}_{0}\eta} \tag{1.5}$$

Photons

A photon is a kind of particle of light that is defined as a distinct bundle of electromagnetic, or light, energy. At all times, photons move at the speed of light in a vacuum, which is just empty space. The speed at which photons travel is c = 2.998 $\times 10^{8}$ m s^{-1}, also referred to as the vacuum speed of light (or just the speed of light) [13].

Protons

A proton is a positively charged subatomic particle that is found in the nucleus of an atom. Its mass is around 1836 times that of an electron, and its charge is +1. Three quarks, one down and two up, make up a proton, which is bound together by the strong nuclear force. Since an element is defined by the amount of protons in its nucleus, they are crucial for ascertaining its identification. Protons, which Ernest Rutherford discovered in 1917, are essential to the composition of matter and are important to both atomic and nuclear physics [14].

Electrons

A negatively charged subatomic particle that circles an atom's nucleus is known as an electron in physics. It has a mass of approximately 1/1836 that of a proton and a charge of -1. Being fundamental particles, electrons don't consist of smaller particles. Electrical conductivity and chemical bonding depend on them. Electrons were discovered in 1897 by J.J. Thomson and are fundamental to the structure of atoms and their interactions, serving as the foundation for a large portion of physics and chemistry [14].

Heavy ions

The cores of heavy atoms without their electrons are known as heavy ions in physics. They weigh a great deal more than elementary particles like protons. Scientists conduct experiments with heavy ions to investigate the fundamental characteristics of matter and the early conditions of the universe. Because heavy ion beams can target and destroy tumor cells accurately, they are also utilized in medicine, especially in the treatment of cancer [2].

1.4 Natural sources of radiation

Cosmic radiation

Ionizing radiation is emitted when alpha particles and photons from outer space interact with the components of the earth's atmosphere, resulting in cosmic radiation. Protons make up the majority of cosmic rays, although they can also be other particles or wave energy. Natural radiation exposure occurs when ionizing radiation enters the earth's atmosphere and is absorbed by humans. They travel at nearly the speed of light, or about 300,000 kilometers per second. Cosmic radiation is divided into two types: galactic and solar. During the supernova explosion of a big star, galactic radiation is emitted. During an explosion, highly penetrating and powerful energy is emitted. This radiation has an ongoing effect on the Earth's surface. Solar cosmic radiation is produced by the sun as a result of a continuous helium reaction in the form of helium. The sources of those radiation is depicted in Figure 1.2 [15], where both solar and cosmic radiation are being blocked by earth magnetosphere. But being so energetic some rays penetrates earth different layers and reach into earth atmosphere [16] .

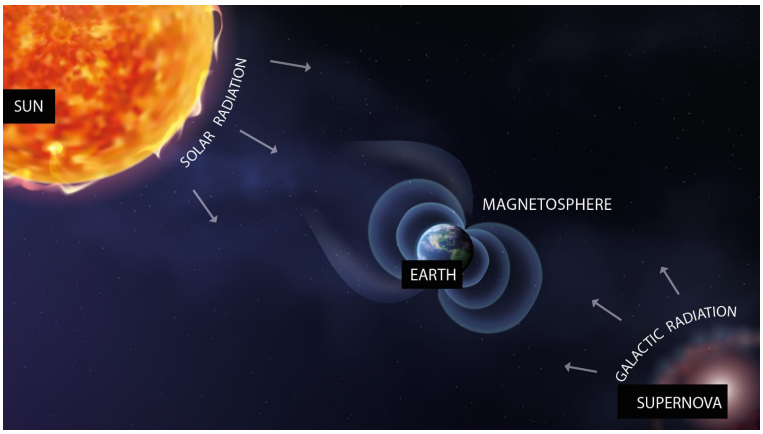

Figure 1.2: Sources of ionizing radiation in interplanetary space.

Terrestrial radiation

Natural radioactive chemicals, which are found all over the world, release this form of radiation. Natural uranium, potassium, and thorium, which decay naturally and generate modest amounts of ionizing radiation, are the principal contributors. People who are exposed to this radiation for an extended period of time may develop major health problems. As a result, radiation shielding may be beneficial in reducing the damaging effects of these rays [17].

Air

Many radioactive minerals naturally occur in soil, mining, and construction materials, which decay to produce radiation and move into the atmosphere as gases, eventually reaching the human body by breathing. When uranium-238 decays, it produces radon, a colorless and odourless gas that is generally innocuous. Also known as thoron, thorium breakdown produces a radioactive gas. Excessive exposure to these radioactive gases has the potential to cause cancer in humans. As a result, persons working in mines, farms, and construction sites, among other places, are at a high risk. As a result, long-term exposure to those locations should be avoided, or appropriate shielding material should be used while working [18].

Food

As we all know, our farmland is utilized to grow vegetables and rice, and water is required for irrigation. Naturally occurring radioactive materials such as carbon-14 and potassium-40 are found in soil and water, and when consumed, result in internal radiation exposure. Excessive exposure can harm deoxyribonucleic acid (DNA) and ribonucleic acid (RNA) as well as soft tissue body parts [19].

1.5 Artificial source of radiation

Medical sources

Radiation is used in medicine to diagnose disorders (e.g. X-ray, CT scan) and to treat and diagnose cancer. This radiation has an impact on both the patient and the radiologist. The most effective strategy to limit patient risk in radiological examinations is to perform suitable tests and make the best use of the patient's radiological protection resources. These are primarily the radiologist's, nuclear medicine clinician's, and health physicist's responsibilities. Figure 1.3 [20] enlighten the uses of teletherapy machine in diagnosis of diseases which uses high amount of radioactive sources to produce radiation. The incoming radiation might cause radiation hazard to front-line health workers as well as patient [21].

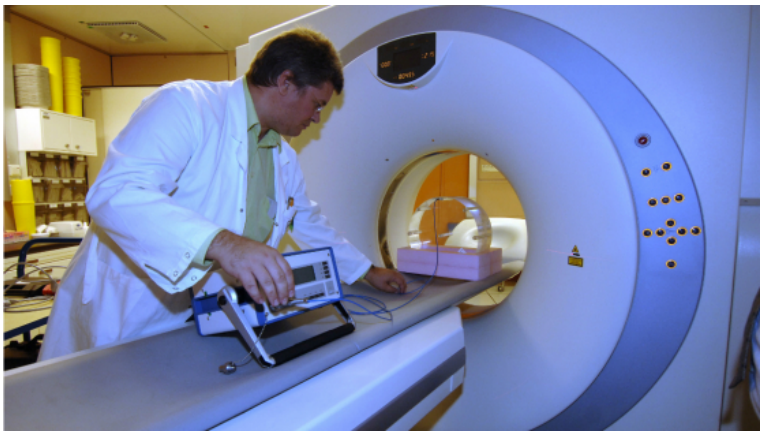

Figure 1.3: Teletherapy machine.

Industrial sources

Industrial radiation sources, including radioactive materials and equipment, are common in industries like food irradiation, materials testing, power generation, and medical imaging. Proper handling and safety procedures reduce risks. Many industrial instruments rely on radioactive sources to determine moisture content, thickness, and other process characteristics. When radioactive sources disintegrate, they emit damaging radiation such as gamma rays, neutrons, and alpha particles, among other things [22].

Nuclear laboratories

There are numerous nuclear research laboratories around the world. Because of the significant use of radioactive material, which produces radiation when it disintegrates, many scientists, engineers and workers in nuclear laboratories are at high risk of toxic

ionizing radiation. In humans, these rays create major health problems. As a result, employees working in such laboratories should be aware of the radiation and take precautions. Radiation shielding may be useful in reducing radiation exposure to humans by decreasing certain radiations [23].

Atmospheric testing

In this atomic era many countries are building nuclear weapons and they tested it in our atmosphere which is also main cause for contamination of radioactive material in world. In nuclear testing radioactive substances like ^{14}C, ^{137}Cs and ^{90}Sr are mostly emitted which are deposited in marine environment as well as in air as radioactive gases [24]. Under inhalation it produce a serious health issue to human as well to marine livings beings.

1.6 Radiation interaction with matter

Radiation can interact with matter through various processes, depending on the type of radiation and the properties of the material it encounters. There are several fundamental interactions that can occur when ionizing radiation interacts with matter:

Photoelectric effect

In 1887, Heinrich Hertz made the first observation of the photoelectric effect. Albert Einstein later explained this phenomena in 1905, and as a result, he was awarded the Nobel Prize in Physics in 1921. When a material is exposed to electromagnetic radiation, which usually takes the form of light or other photons, it releases electron. The photoelectric effect is given by Einstein which is shown in Eq.(1.6) and Schematic illustration of photoelectric effect shown in Figure 1.4 [25].

$$E = h\nu = \phi + \text{K.E.} \tag{1.6}$$

where:

- E is the energy of the incoming photon.
- h is Planck's constant (6.63×10^{-34} J s).

- ν is the frequency of the incoming light.
- ϕ is the work function of the material (the minimum energy required to remove an electron from the material's surface).
- K.E. is the kinetic energy of the emitted electron.

Rearranging this equation, we get:

$$\text{K.E.} = h\nu - \phi \tag{1.7}$$

This shows that the kinetic energy of the emitted electrons depends on the frequency of the incident light and the work function of the material. If the energy of the incoming photons is greater than the work function, electrons will be emitted, and the excess energy will be converted into the kinetic energy of these electrons.

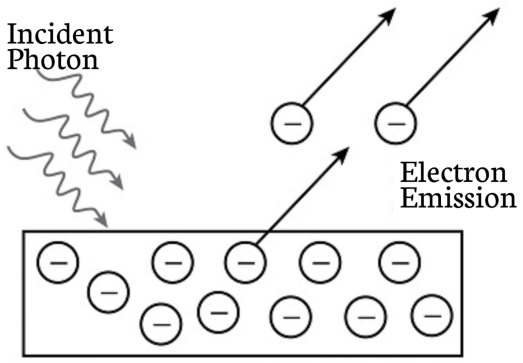

Figure 1.4: Schematic illustration of photoelectric effect.

Compton effect

Compton scattering, another name for the Compton effect, is a basic physics phenomena that explains how electrons scatter high-energy photons, such as gamma or X-rays. When Arthur Compton made the discovery in 1923, it offered compelling proof that light behaves like a particle.

This is how it happens: an electron receives a portion of the energy and momentum that a high-energy photon imparts to it upon collision. The photon changes in wavelength (or energy) as a result of this impact because it scatters at an angle that differs from its initial direction. The angle of scattering determines how much momentum and energy are

delivered to the electron. Schematic illustration of Compton effect is shown in Figure 1.5 [26].

The equation of the Compton effect is given by the Eq. (1.8).

$$\Delta\lambda = \lambda' - \lambda = \frac{h}{m_e c}(1 - \cos\theta) \tag{1.8}$$

where:

- $\Delta\lambda$ is the change in wavelength.
- λ is the initial wavelength of the photon.
- λ' is the wavelength of the scattered photon.
- h is Planck's constant (6.63×10^{-34} J s).
- m_e is the rest mass of the electron (9.11×10^{-31} kg).
- c is the speed of light in a vacuum (3×10^8 m s^{-1}).
- θ is the scattering angle of the photon.

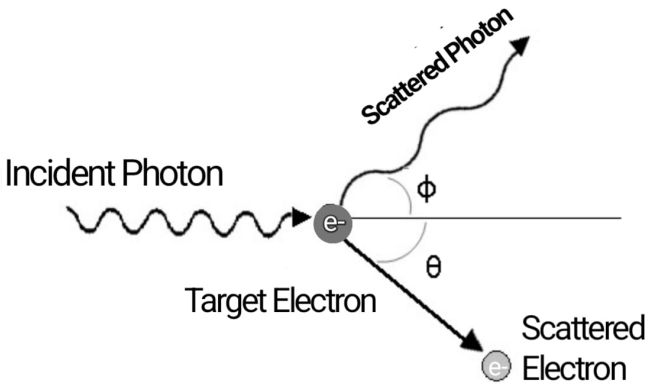

Figure 1.5: Schematic illustration of Compton effect.

Pair Production

A gamma-ray photon, a high-energy photon, interacts with a nucleus or another particle to produce a particle-antiparticle pair. This process is known as pair creation and is a fundamental one in particle physics. Einstein's equation E = mc^2, which allows energy (E) to be converted into mass (m) and vice versa, governs this process [27]. Pair production is a quantum phenomenon in which a gamma-ray photon, with sufficient energy, is

converted into an electron-positron pair when it interacts with the electromagnetic field of a nucleus or an electron. Schematic illustration of pair production process shown in Figure 1.6 [28]. The energy requirement for pair production is given by the Eq. (1.9).

$$E_\gamma \geq 2\mathrm{m_e c^2} \tag{1.9}$$

where:

- E_γ is the energy of the gamma-ray photon.
- m_e is the rest mass of the electron (and positron), 9.11×10^{-31} kg.
- c is the speed of light in a vacuum, 3×10^8 m s^{-1}.

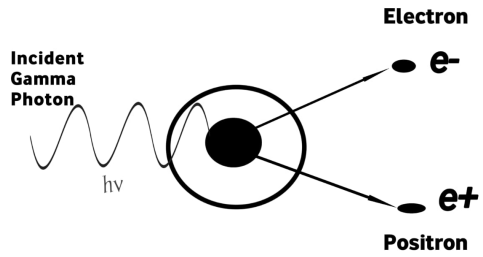

Figure 1.6: Schematic illustration of pair production process.

Triplet production

When three charged leptons, like as taus, muons, or electrons, are produced simultaneously in high-energy collisions or interactions, it's known as triplet formation. It aids in the study of particle interactions and characteristics at extremely high energies, enabling physicists to gain understanding of the basic basis of forces and matter [29]. Triplet production is a process where a high-energy photon interacts with an atomic electron, producing an electron-positron pair while the original electron remains free. The energy requirement for triplet production is given by the Eq. (1.10).

$$E_\gamma \geq 4\mathrm{m_e c^2} \tag{1.10}$$

where:

- E_γ is the energy of the incoming photon.

- m_e is the rest mass of the electron (and positron), 9.11×10^{-31} kg.
- c is the speed of light in a vacuum, 3×10^8 m s^{-1}.

1.7 Photoelectric absorption

When an incident photon interacts with the atom during photoelectric absorption, an electron is released from one of the inner shells of the atom. This phenomenon is most noticeable at photon energies that are just a little bit higher than the electron's binding energy in its shell. Because photoelectric absorption is highly dependent on the atomic number of the material, it is essential for radiation shielding and X-ray imaging applications [30].

1.8 Compton scattering

When an incident X-ray or gamma photon collides with a loosely bound electron, a phenomenon known as Compton scattering occurs. This energy transfer results in the photon scattering at a lower energy (longer wavelength) and the electron recoiling. This phenomenon is frequently employed in many domains, including as particle physics, astrophysics, and medical imaging, and is important in understanding the dual nature of light [31].

1.9 Radiation shielding

Any material that absorbs or filters harmful radiation emitted by radiating sources and protects against it is referred to as radiation shielding. The concept of radiation shielding was developed to protect people from the harmful effects of radiation on their health. Food preservation, radiotherapy, nuclear laboratories, spaceships, aircraft, and industrial radiography are all examples of settings where individuals are directly exposed to hazardous radiation [32].

Protection from radiation

Radiation protection entails limiting exposure to dangerous ionizing radiation by keeping a safe distance, managing your time, and using shielding. Geiger counters and lead

aprons are examples of personal protective equipment that helps monitor and lower exposure. In locations where radiation is present, like medical facilities and nuclear power plants, regulatory standards are essential for guaranteeing worker safety. Fundamental ideas in radiation protection can be illustrate as in Figure 1.7 [28]. Since radiation poses a risk to human health, it needs to be protected. The three fundamental ideas of radiation protection are shielding, time, and distance [33].

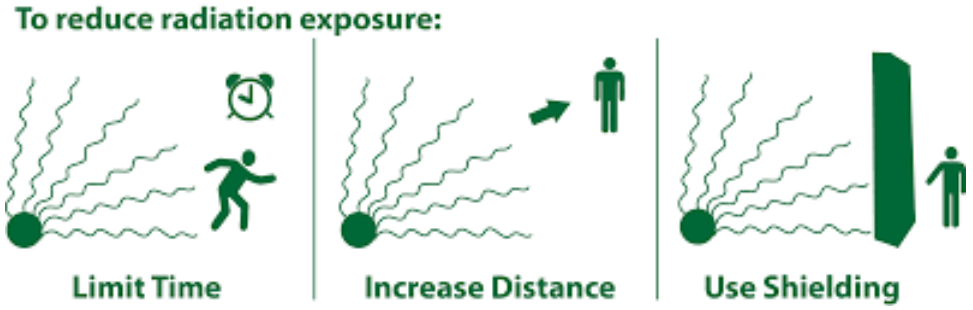

Figure 1.7: Fundamental ideas in radiation protection.

1.10 Effect of radiation

Natural or artificial radiation can have both positive and negative effects on the environment. For instance, both positive and negative impacts of light can be seen in plant and animal life. In little doses, radiation can be good for the environment. On the other hand, ionized radiation, such as X-rays, gamma rays, alpha and beta particles, can be seriously harmful at high doses. The effects of radiation on the planet can be dangerous and deadly to people, animals, and plants. The amount of radiation and the organism's resistance determine how much harm is caused. Molecules are obliterated by radiation because they lose electrons. You can become ill by merely blocking certain of the body's enzymes. However, the body might not be able to heal itself if radiation damages Deoxyribonucleic Acid (DNA). As a result, cancer is a risk that affects both people and animals [34].

Chapter 2

Literature Review

Many researchers throughout the world have been drawn to developing the best radiation shielding materials and studying their qualities in terms of shielding harmful radiation through experimental and theoretical methods. In addition, alternative programs and software are being developed to better comprehend the chemical, optical, physical, and other aspects of various materials. The following is a list of some of the most important research projects in this topic.

Bantan et al. (2020) [35] studied about the gamma ray shielding capacity of various natural rocks and found that Basalt-1 rock have highest shielding capacity. Some natural rocks may be able to provide an adequate substitute for conventional shielding materials when it comes to gamma ray shielding. This finding could lead to additional studies and applications in a variety of industries. Through the integration of theoretical calculations, Monte Carlo simulations, and experimental data, the authors have established a standard for future investigations seeking to investigate and optimize natural materials for shielding applications.

Obaid et al. (2018) [36] studied shielding parameters on rocks and concrete and they found that, for gamma ray shielding purposes, feldspathic basalt, compact basalt, volcanic rock, dolerite, and pink granite are more effective than sandstone and concrete.

Obaid et al. (2018) [37] investigated the attenuation coefficients of some rocks for γ-ray shielding applications and show that the pink stone exhibits the best shielding qualities

against γ-ray radiation among the examined samples. Their study was conducted to investigate the potential benefits of using the chosen rocks in engineering structures and building construction as a means of shielding γ-radiation.

Akkurt et al. (2007) [38] studied the characteristics of various igneous rocks for γ-ray shielding using XCOM software and found photon linear attenuation coefficients (μ) were determined for four igneous rocks used in industry. Findings indicated that as coefficients increased, there was a decrease in porosity and abrasion strength and an increase in density, compressive strength, bending strength, shore hardness, and SiO_2 percentage.
Waly et al. (2019) [39] studied the structural and nuclear radiation shielding properties of bauxite ore doped lithium borate glasses found that lithium borate glasses shielding qualities have been enhanced by the metals Fe, Ti, and Al found in the bauxite mine.

Issa et al. (2016) [40] studied the gamma radiation shielding efficiency of zinc tellurite glasses. They found mass attenuation coefficients were satisfactorily agree with the theoretical values obtained using WinXCom. The effective atomic numbers and electron densities were found to be the highest for a 40ZnO-60TeO_2 glass in the energy range of 0.04 – 0.2 MeV. The 10ZnO - 90TeO_2 glass sample had lower values of gamma ray exposure buildup factors in the intermediate energy region.

Durante et al. (2011) [41] studied about the radiation protection in space travel. Their research found that radiation in space, in the form of heavy ion charge particles, is more energetic and penetrating than radiation on Earth. According to the findings, passive shielding is better for solar radiation but not for galactic cosmic rays (GCR). As a result, they concentrate on genetic and biological approaches, as well as inventing suitable shielding material for space radiation, to protect ourselves from GCR.

Islam et al. (2020) [42] examined the radiation shielding parameters of bees-wax and their effectiveness in cancer treatment as bolus material. They used MNCP5 code for calculation of photon attenuation parameter in energy range 15keV to 10 MeV. The result shows that bees-wax radiation shielding properties is equivalent to water as well as

body tissue. Also bees-wax can be used in treatment of cancer patient as bolus material.

Hadeethi et al. (2021) [43] studied about WO_3-ZnO-PbO-B_2O_3 glasses using Geant4 and Phy-X/PSD simulation. They looked at seven samples of glass alloys with varying compositions and densities ranging from 2.75 to 4.03 (g cm^{-3}), and discovered that the transmission factor decreases as the thickness increases from 0.2 to 1 cm. They chose a range of energies between 0.12 and 1.46 MeV. They conclude that when the energy value increases, the capacity for shielding radiation diminishes. They also discovered a positive impact of density on *LAC* values, implying that the higher the density, the greater the radiation shielding capacity of glass samples.

Kilic et al. (2020) [44] measured the radiation shielding properties of novel zinc vanadyl boro-phosphate glasses (ZnO-V_2O_5-P_2O_5-B_2O_3) having five different composition using MNCP code and XCOM software. They prepared five glass samples with density ranging from 2.81 g cm^{-3} to 2.89 g cm^{-3}. They selected suitable energy range from 15 keV to 15 MeV to calculate different radiation attenuation parameters. They found glass with 0.01 mol % ZnO has the lowest *LAC* values that ranged from 43.01 cm^{-1} at 15 keV to 0.06 cm^{-1} at 15 MeV, while glass with the highest ZnO ratio (8.0 mol %) has maximum *LAC* ranged from 50.52 cm^{-1} to 0.07 cm^{-1}. They also calculated other shielding parameter and result showed that selected glasses can be used as radiation shielding material and concluded that the glass with higher concentration of ZnO have best shielding properties than other selected samples.

Qian et al. (2021) [45] investigated the gamma ray shielding properties of lead boro-telluro-phosphate glasses with Sm^{3+} doped and effect of adding PBO content on it. They use MCNP5 simulation code and XCOM software to calculate different shielding factors. The result showed increase in shielding capacity as content of PbO is increased and shielding capability is maximum for $20B_2O_3$-40PbO-$14TeO_2$-$10P_2O_5$-7.5BaO-7.5CdO-Sm_2O_3 glass alloy which has highest % (i.e. 40%) of PBO content in mol among selected samples. They were taken energy range from 0.02 MeV to 10 MeV.

Sayyed et al. (2021) [46] experimentally determined the radiation shielding features of

CaO-K_2O-Na_2O-P_2O_5 glass systems in energy range 59.5 keV to 1.41 MeV and compared with theoretical value obtained from XCOM. They found maximum Z_{eff} values (12.41-12.55) at minimum energy (59.5 keV) later it decreases to 10.69-10.80 at 0.25 MeV. Also lowest value of mean free path was obtained in lowest energy 59.5 keV and the radiation protection efficiency (RPE) value reflect that decreasing the P_2O_5 content in the glasses enhance the radiation shielding ability of the samples.

Bashter et al. (1997) [47] performed theoretical calculations to determine the mass and linear attenuation coefficients for several types of concrete: ordinary, hematite-serpentine, limonite-limenite, basalt-magnetite, ilmenite, steel-scrap, and steel-magnetite. The results showed that the computed and measured values were consistent, and it was found that steel-magnetite concrete, which has a high density and atomic number, functions effectively as a shield against photons and neutrons.

Upadhyay et al. (2023) [48] evaluated the radiation shielding performance of five quaternary glass systems with different chemical compositions of $60SiO_2$-$35Pb_3O_4$-(5-x) ZnO-xWO_3 using theoretical software and Monte Carlo simulations. PZSW3 and PZSW5 show comparable attenuation coefficients and neutron removal cross-sections, but PZSW5 exhibits greater radiation attenuation and the most effective radiation protection capability among the glass composites studied.

Dulal et al. (2024) [49] analyzed the silver tellurite glasses attenuation properties against ions, neutrons, and gamma rays as well as against other forms of ionizing radiation. The study uses advanced computational tools such as the PHITS Monte carlo method and theoretical software like Phy-X/PSD and NIST XCOM to simulate and compute various shielding parameters. Among them are the effective atomic number, the effective electron density, and the build-up parameters for energy absorption. A few of the ways that radiation interacts with glass materials are through the photoelectric effect, pair creation, and Compton scattering.

2.1 Research gap / motivation

After reviewing all these literature, we came into conclusion that estimation of radiation shielding properties of rocks used in Nepal is also necessary. Nowadays, nuclear physics techniques are being applied more and more to material science, so my attention was drawn here. The Chernobyl radiation leak catastrophe in 1986 and the Fukushima nuclear accident in 2011 have brought attention to the urgent need for precise and thorough study on the resilience and effectiveness of building materials used as radiation shields. In Nepal, the majority of dwellings are built of rocks. Investigating the effectiveness of rocks as radiation protection is crucial. Radiation shielding is the practice of protecting people and the environment from the harmful effect of ionising radiation [2]. So it is very sensitive issue for our environment and human civilization. Due to various radiation peoples are suffering from long-term health impact, such as cancer and heart disease. Low-level radiation exposure in the environment has no immediate effects on our health, but it does contribute to our overall cancer risk. Our research concern is to create a idea to protect people from harmful ionizing radiation. For this shielding is the best way, to design and manufacture the best shielding material capable of blocking heavy ion charged particles. It's most useful for space travel because it shields astronauts from harmful radiation.

2.2 Objectives

The general objective is:

- To determine the radiation shielding properties of the natural rock samples.

Our specific objectives are:

- To estimate the physical and chemical composition of the rocks samples using Archimedes principles and Inductively coupled plasma optical emission spectrometer (ICP-OES).
- To analyze radiation shielding parameters such as mass attenuation coefficient (*MAC*), linear attenuation coefficient (*LAC*), half value layer (*HVL*), tenth value layer (*TVL*), effective conductivity, electron density, effective atomic number, mean free path using Phy-X/PSD.
- To study fast neutrons removal cross section of rock samples.
- To study photon trajectory and dose distribution using Particle and Heavy Ion Transport code System (PHITS).

Chapter 3

Materials & methods

3.1 Materials

3.1.1 Study area

Nepal is a South Asian nation with a varied geography, mostly found in the Himalayas. The low-lying Terai plains, which are only 60 meters above sea level, and the lofty Himalayan highlands, which include Mount Everest, the highest point on Earth at 8,848.86 m. Nepal lies at the 3265 m above the sea level and covers the area of about 1,47,516 km^2. Figure 3.1 represent the map of Nepal with study area from where sample was collected this map is generated by ArcGIS 10.4.1.

Figure 3.1: Map representing study area.

Table 3.1: Five different co-ordinates from where samples were taken.

S.N.	Location name	Sample name	Latitude (degree)	Longitude (degree)	Altitude (m)
1	Sindhupalchok	Quartz-I	27.81972	85.78198	1000
2	Lalitpur	Phyllite	27.55407	85.31802	1600
3	Baitadi	Granite	29.63975	80.51197	700
4	Bajura-A	Quartz-II	29.38764	81.37881	1012
5	Bajura-B	Sandstone	29.37362	81.35282	1011

3.1.2 Samples collection

Five distinct samples of rocks (Quartz-I, Phyllite, Granite, Quartz-II and Sandstone) were gathered from the research region. The samples were randomly selected from five different districts, and the coordinates (longitude, latitude, and altitude) of each sample collection are recorded. Every sample had a proper label after being delivered to the lab as shown in Figure 3.2.

Figure 3.2: Sample collection and labeling in laboratory.

3.1.3 Samples preparation

We follow the following process to preparing the sample [50].

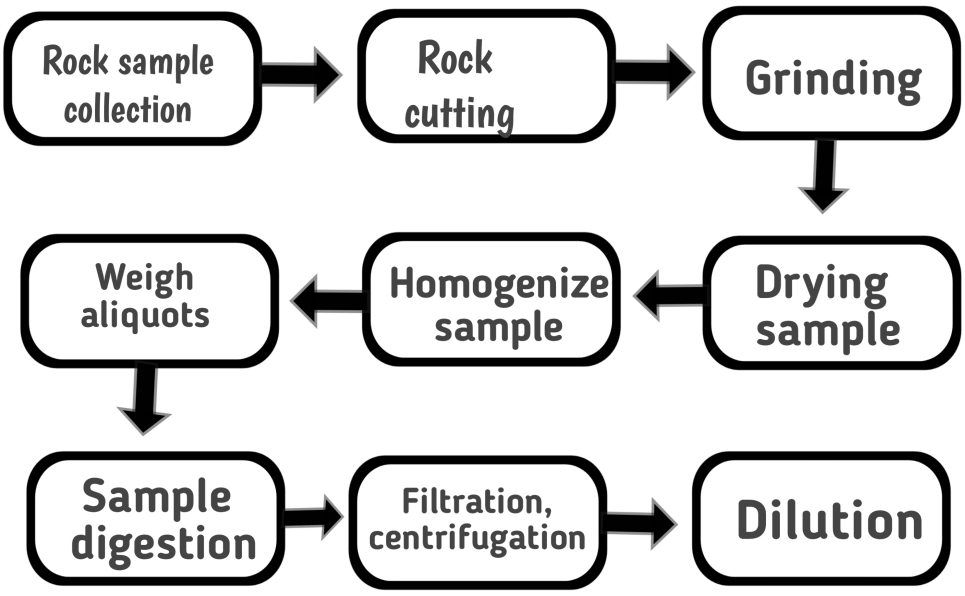

Figure 3.3: Generalized rocks sample preparation process.

To measure the attenuation parameters experimentally, each sample was chopped into three distinct thicknesses. The following Table 3.2 and Table 3.3 displays the plates with varying thicknesses.

Table 3.2: Thickness and density of five different samples taken.

S.N.	Location name	Sample name	Thickness (mm)	Density (g cm^{-3})
1	Sindhupalchok	Quartz-I	31.67	2.58
2	Lalitpur	Phyllite	28.81	2.67
3	Baitadi	Granite	30.66	2.81
4	Bajura-A	Quartz-II	12.65	2.67
5	Bajura-B	Sandstone	31.51	2.48

(a) **(b)**

(c) **(d)**

Figure 3.4: (a) Measuring thickness of rocks. (b) Making fine plate sheet with the help of rock-cutter. (c) Stored prepared sample in laboratory with proper labeling. (d) Making fine powder.

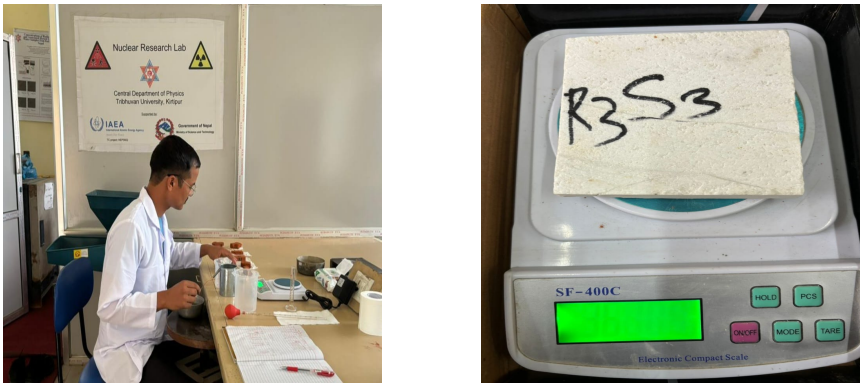

(a) **(b)**

Figure 3.5: (a) Measuring density of rocks sample. (b) Measuring the weight of rock sample.

Using a grinder, we reduced the stone to a fine powder in order to do an experimental determination of its chemical composition.

Table 3.3: Table shows the prepared samples in different form .

Sample name	Before preparation	After preparation	Powder form	Dilution
Quartz-I				
Phyllite	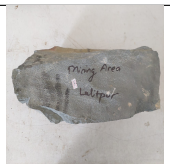			
Granite	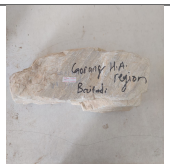			
Quartz-II	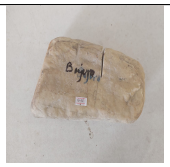			
Sandstone		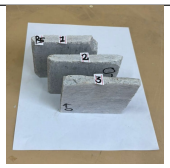		

3.1.4 Method

3.1.5 Inductively coupled plasma optical emission spectroscopy

Introduction

An analytical method called Inductively Coupled Plasma Optical Emission Spectroscopy (ICP-OES) is used to identify and measure the elemental makeup of a variety of materials. The technique uses an inductively coupled plasma to excite atoms and ions in a sample, causing them to release light at particular wavelengths. An optical emission spectrometer then examines the light that has been released in order to calculate the elemental concentration. Because of its high sensitivity, capacity to analyze many components at once, and quick analytical capabilities, ICP-OES is widely used in environmental analysis, food safety, pharmaceuticals, and metallurgy. However, because of its high operating expenses and skill requirement, it requires skilled operation. Typical components of an ICP-OES system shown in Figure 3.6(a) [50].

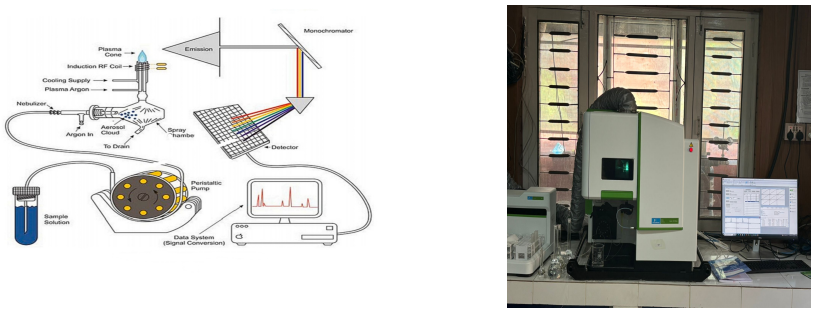

(a) **(b)**

Figure 3.6: (a) Typical components of an ICP-OES system. (b) ICP-OES instruments in lab.

Working steps of ICP-OES

- When the Argon gas passing through, the quartz tube is sparked, it generates argon ions,
- These argon ions are positively charged,
- The radio frequency (RF) coil generates oscillating magnetic field,
- This causes Acceleration of argon ions,
- The argon ions collides with other argon atoms to generate more other argon ions,
- The ionized gas so formed is known as Plasma,
- Plasma, has temperature about 6000 K,
- when the sample molecules/atoms are allowed to enter the Plasma, they emit radiation (Emission spectra),
- Detector detects this radiation (wavelength),
- Information is analyzed by computer & finally displayed.

Sample testing in laboratory

Well prepared sample for testing the chemistry of the rocks sample are shown in Figure 3.7(a) and sample testing work conducting in Figure 3.7(b).

(a) (b)

Figure 3.7: (a) Sample prepared for ICP-OES. (b) Sample testing in ICP-OES.

3.1.6 Theoretical method

3.1.7 Phy-X/PSD

For the calculation of different radiation attenuation parameters we use Phy-X/PSD software which is shown in Figure 3.8 [51]. This is work within the energy range 0.015 MeV to 15 MeV. Obtained data is plotted using Python programming.

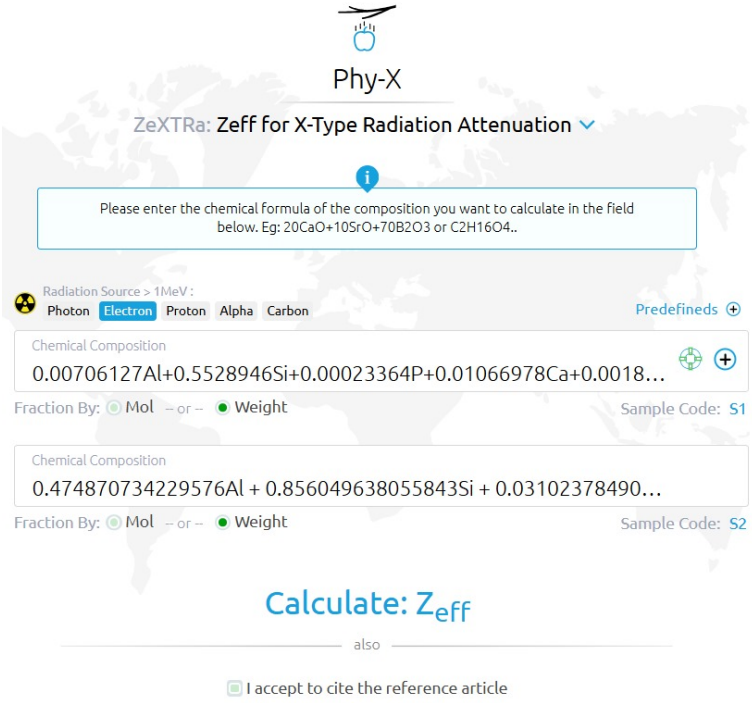

Figure 3.8: Phy-X/PSD online software.

3.2 PHITS

The widely used Monte Carlo particle transport simulation code PHITS was created in collaboration with the JAEA, RIST, KEK and several other organizations. It makes use of several nuclear reaction models and nuclear data libraries to manage particle mobility across a broad energy range. Monte Carlo method trace each particle motion using random number, and estimate their average behaviour by iterating the simulation. Monte Carlo simulation is a mathematical technique that generates random variables for modelling risk or uncertainty of a certain system. The random variables or inputs are modelled on the basis of probability distributions such as normal, log normal etc. Various applications of PHITS in different fields shown in Figure 3.9 [52].

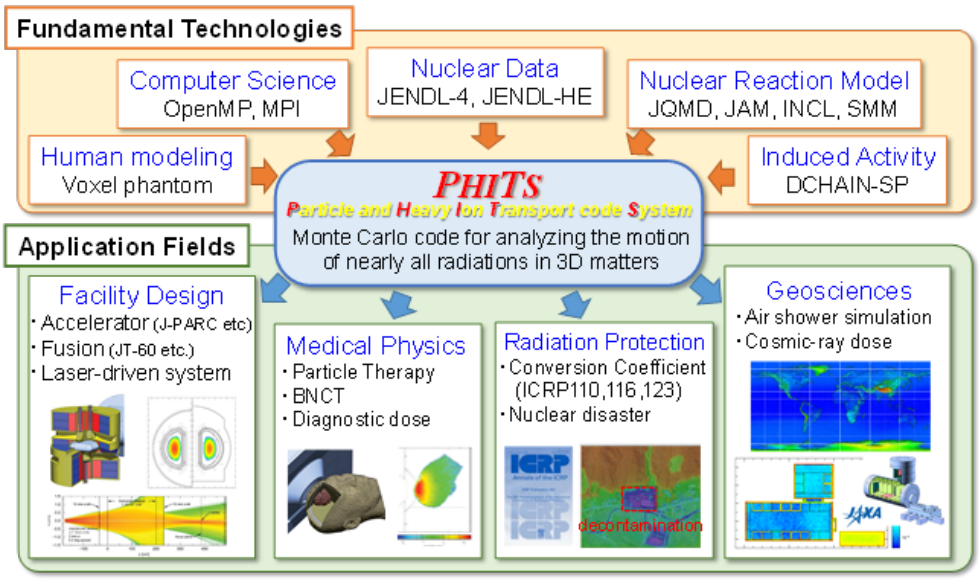

Figure 3.9: Particle and heavy ion transport code system tool.

3.3 Theoretical and conceptual framework

Theoretically, the radiation coefficient are calculated using following formulas:

Beer Lambert Law

The mass attenuation coefficient (*MAC*) (μ_m) is a quantity that describes the interaction probability between photons and the mass per unit area for a certain medium and can be calculated by the well-known Beer Lambert law given in Eq. (3.1) and *MAC* is calculated

using Eq. (3.2) [53].

$$I = I_0 e^{-\mu t} \tag{3.1}$$

$$\mu_m = \left(\frac{\mu}{\rho}\right) = \frac{\ln(I_0/I)}{\rho t} \tag{3.2}$$

where I_0 and I are un–attenuated and attenuated photon intensities, μ (cm^{-1}) and μ_m (cm^2 g^{-1}) are linear and mass attenuation coefficients, t (cm) and ρ(g cm^{-3}) are the thickness and density of material. For mixture and compound we use Eq. (3.3)

$$\mu_m = \left(\frac{\mu}{\rho}\right) = \sum_i W_i \left(\frac{\mu}{\rho}\right)_i \tag{3.3}$$

where w_i and $(\mu/\rho)_i$ are the weight fraction and the mass attenuation coefficient of the i^{th} constituent element respectively.

Linear attenuation coefficient

Linear attenuation coefficient (*LAC*) is calculated by using the Eq. (3.4) [54].

$$\mu = \left(\frac{1}{t}\right) \ln(I_o/I) \tag{3.4}$$

where t is the thickness of the rock.

Mass attenuation coefficient

Mass attenuation coefficient (*MAC*) is calculated by using the Eq. (3.5) [55].

$$MAC = \frac{\mu}{\rho} \tag{3.5}$$

where ρ is the density of the rock.

Mean free path

Mean Free Path (*MFP*) is another factor affecting radiation shielding properties which is defined as the average distance that a particle (atom, molecule, photon) travels between

successive collisions with other particles. *MFP* is calculated using Eq. (3.6) [56].

$$MFP = \frac{1}{\mu} \tag{3.6}$$

where μ is linear attenuation coefficient.

Half value layer

Half value layer (*HVL*) is important factor in determining the shielding characteristics of the material with respect to its thickness per unit. *HVL* denotes the thickness that decreases 50% of the radiation passing through the material. Eq. (3.7) is used to determine *HVL* value [57].

$$HVL = \frac{\ln(2)}{\mu} \tag{3.7}$$

Tenth value layer

The tenth value layer (*TVL*) defines the thickness of the material that decreases the radiation passing by a factor of one tenth of the initial value. The Eq. (3.8) is for determination of *TVL*.

$$TVL = \frac{\ln(10)}{\mu} \tag{3.8}$$

Radiation protection efficiency

The ability of the shielding materials to attenuate incident photons is measured by the radiation protection efficiency (*RPE*), which is computed using the Eq. (3.9) [58]

$$\mathrm{RPE} = 1 - \mathrm{e}^{-\mu \mathrm{x}} \tag{3.9}$$

where x is the thickness of the rock.

Atomic cross section

Total atomic cross section (*ACS*) is the sum of all cross section by which electron interacts with the atom. *ACS* can be evaluated from given Eq. (3.10) [55].

$$ACS = \frac{(\mu/\rho)_{alloy}}{N_A \sum_i \frac{w_i}{A_i}} \tag{3.10}$$

where A_i, w_i is the atomic weight and weight fraction of each element in the mixture.

N_A is Avogadro's Number.

Electronic cross Section

Total electronic cross section (*ECS*) is the cross section by which electron interacts with the photon. Eq. (3.11) determines the *ECS* value.

$$ECS = \frac{1}{N_A} \sum_i \frac{F_i A_i}{Z_i} \left(\frac{\mu}{\rho}\right)_i \tag{3.11}$$

where Z_i, F_i, $(\mu/\rho)_i$ and A_i are the atomic number, mole fraction, mass attenuation coefficient and atomic weight of the i^{th} constituent element, respectively.

Effective atomic number

For a material composed of different elements such as glasses, it is appropriate to deal with another quantity called effective atomic number (Z_{eff}). It is computed using the Eq. (3.12) [54].

$$Z_{\text{eff}} = \frac{\sum_i F_i A_i (\mu/\rho)_i}{\sum_j F_j (A_j/Z_j)(\mu/\rho)_j} = \frac{ACS}{ECS} \tag{3.12}$$

Effective electron density

Effective electron density (N_{eff}) is number of electrons per unit mass of the interacting materials and measured in electrons/g. Eq. (3.13) is used to calculate effective electron density [59].

$$N_{\text{eff}} = \frac{\mu_m}{ECS} \tag{3.13}$$

where μ_m is the mass attenuation coefficient and *ECS* is electronic cross section.

Effective conductivity

Effective conductivity (C_{eff}) of glass material is related to effective electron density (N_{eff}) through Eq. (3.14) [59].

$$C_{\text{eff}} = \left(\frac{N_{\text{eff}} \rho \tau e^2}{m_e}\right) 10^3 \tag{3.14}$$

where e and m_e are charge and mass of electron, respectively. τ is the average life time of the electron at the Fermi Surface.

Fast neutrons removal Cross Section

Fast neutrons removal cross section (*FNRCS*) gives information about neutrons attenuation potential of any given material.*FNRCS* ($\sum_R$) is determined using Eq. (3.15).

$$\sum_R = \sum_i \rho_i \left(\frac{\sum_R}{\rho} \right)_i \tag{3.15}$$

where, ρ_i and $(\frac{\sum_R}{\rho})_i$ are the partial density and mass removal cross-section of the i^{th} constituent respectively [59].

Density of rock

Density of rocks is determined using the Archimedes principle. Three weights are measured on a single specimen in the Archimedes method: w_d, or the dry specimen weight; w_{sat}, or the specimen fully saturated in a liquid (typically water); and w_A, or the saturated specimen suspended and completely submerged in the saturating liquid weight. The Archimedes weight, or w_A, is the final one of these. Eq. (3.16) can be used to derive the density ρ_b from these three quantities [60].

$$\rho_b = \frac{w_d \rho_w}{w_{\text{sat}} - w_A} = \frac{m_d}{V_b} \tag{3.16}$$

here, ρ_w is the density of the water ρ_b bulk density of rock sample.

$$V_b = \frac{(w_{\text{sat}} - w_A)}{\rho_w} \tag{3.17}$$

Here, V_b bulk volume of rock.

3.4 Data analysis

Python programming

The data from gamma-spectrometry was analyzed and compiled using Python computer programming. Representation of Python programming software shown in Figure 3.10 (b) [61]. Python, developed by Guido van Rossum in 1991, is a popular high-level interpreted language suitable for web development, data science, automation, and more due to its ease of learning and vast range of applications.

ArcGIS

Esri's ArcGIS version 10.4.1, a feature-rich GIS, enables spatial analysis, complex map-making, and efficient geographic data management, making it a valuable tool for specialists in mapping, urban planning, and environmental management. ArcGIS version 10.4.1 computer software as shown in Figure 3.10 (a) [62] was used to plot the local base map using different co-ordinate from studied area.

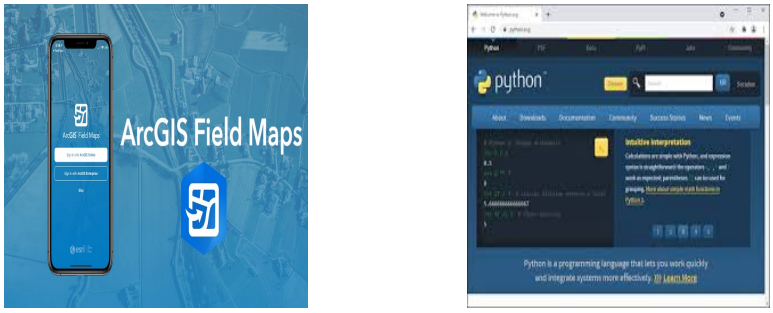

(a) **(b)**

Figure 3.10: (a) Representation of ArcGIS tool. (b) Representation of Python programming software.

Chapter 4

Results and Discussion

4.1 Chemical Composition

The chemical composition and density of our selected five rock samples named as Quartz-I, Phyllite, Granite, Quartz-II and Sandstone are listed in Table 4.1. Inductively Coupled Plasma Optical Emission Spectroscopy (ICP-OES) is used to measure the chemical composition of rock samples because it is an analytical technique used to determine and quantify the elemental composition of a wide range of materials. The density is measured in lab by using Archimedes's principle as described in methodology.

Table 4.1: The chemical composition of the selected rocks.

Element symbol	Chemical composition Wt.%				
	Quartz-I	Phyllite	Granite	Quartz-II	Sandstone
Al	3.86	2.01	1.32	0.39	1.69
Si	69.06	68.68	66.12	65.84	67.89
P	0.29	0.05	0.10	0.09	0.14
Ca	0.30	0.77	0.10	0.15	0.16
Mg	0.19	0.66	0.05	0.04	0.04
Na	0.88	0.49	0.17	0.13	0.16
K	1.11	1.55	0.45	0.08	0.24
Fe	0.46	4.82	0.06	0.15	0.69
Mn	0.01	0.03	0.01	0.01	0.01
Ti	0.11	0.64	0.04	0.03	0.02
Density (g cm^{-3})	2.58	2.67	2.81	2.67	2.81

4.2 Radiation shielding parameter

Mass attenuation coefficients and Linear attenuation coefficient

Phy-X/PSD software with energy range 15 keV to 15 MeV is used to determine radiation shielding parameters using chemical composition of our selected five rock samples and various graphs are plotted based on the data that is obtained. Below is a discussion and analysis of the acquired data and graph types:

Five chosen samples referred to as Quartz-I, Phyllite, Granite, Quartz-II, and Sandstone had their mass attenuation coefficients (*MAC*) determined and plotted on a graph as seen in Figure 4.1(a). The high value of *MAC* obtained for the Phyllite is 6.54 cm^2 g^{-1} and minimum value of *MAC* for Quartz-II is 5.08 cm^2 g^{-1}. According to obtained value of our five sample Phyllite has highest *MAC* value and Quartz-II has lowest value. According to *MAC* value shielding capacity of five sample increases in following order as Quartz-II < sandstone < Granite < Quartz-I < Phyllite. Thus Phyllite has best shielding ability among five sample.

Similarly the linear attenuation coefficient (*LAC*) of five selected samples named as Quartz-I, Phyllite, Granite, Quartz-II and Sandstone was obtained and plotted in graph as shown in Figure 4.1(b). According to obtained value of our five sample Phyllite has highest *LAC* value which is 17.46 cm^2 g^{-1} and Sandstone has lowest value which is 13.42 cm^2 g^{-1}. According to *LAC* value shielding capacity of five sample increases in following order as sandstone < Quartz-II < Granite < Quartz-I < Phyllite. Thus Phyllite has best shielding ability among five sample. The measured value and graph show that the low energy range has the best shielding capacity, with the *LAC* value decreasing by up to 15 MeV as energy increases. In Figure 4.1(b) displays the plotted linear attenuation coefficient (*LAC*) graph for the five samples(Quartz-I, Phyllite, Granite, Quartz-II, and Sandstone) that were chosen. We acquired maximum *LAC* values at low energy and minimum *LAC* values at high energy (15 MeV) for five samples, as we know that *LAC* values rely upon the density of rock samples and *MAC* values.

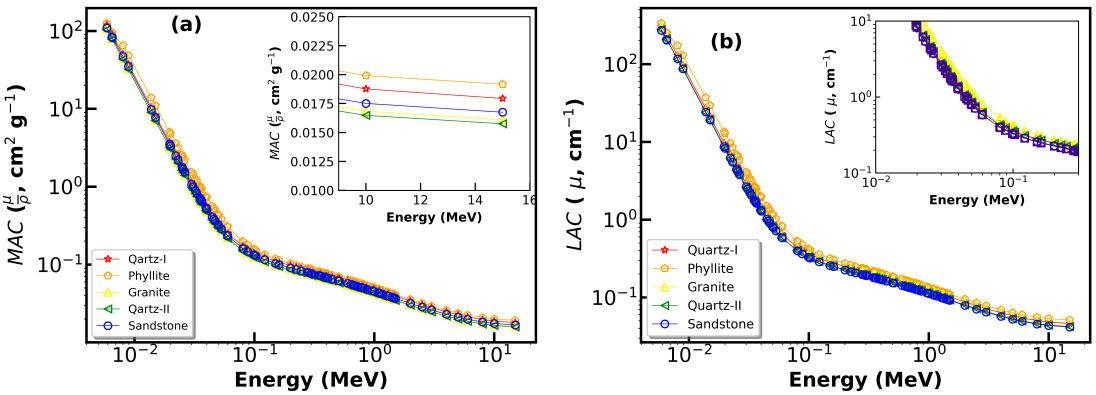

Figure 4.1: (a) Photon energy versus *MAC* of five rocks samples. (b) Photon energy versus *LAC* of five rocks samples.

Half value layer and Tenth value layer

Another important factor for study of penetration of photon radiation is half value layer. The graph for *HVL* is plotted and shown in Figure 4.2 . The graph depicts that the half value layer increases linearly with energy. Also many other previous work indicates that for better shielding capacity the *HVL* should be as small as possible. From obtained data we can conclude that Sandstone has highest *HVL* which is 3.75 cm and Phyllite have lowest *HVL* value which is 3.08 cm , which suggest Phyllite sample contain best shielding properties among our five sample and Sandstone contain least photon shielding properties and represented as sandstone > Quartz-II > Granite > Quartz-I > Phyllite.

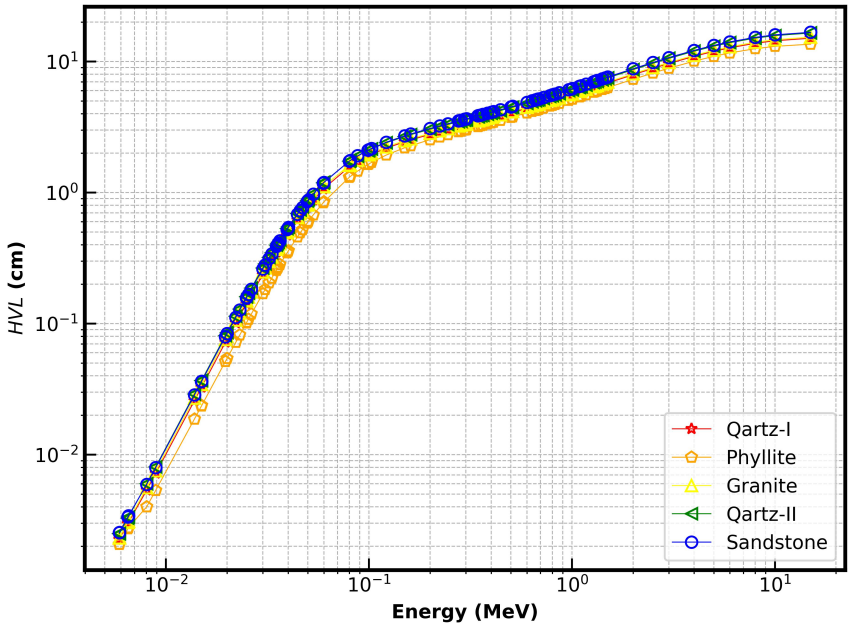

Figure 4.2: Photon energy versus *HVL* of the five rock sample.

Another important factor for study of penetration of photon radiation is the tenth value layer. The graph for *TVL* is plotted and shown in Figure 4.3. The graph depicts that the tenth value layer increases linearly with energy. Also many other previous work indicates that for better shielding capacity *TVL* value should be as small as possible. From obtained data we can conclude that Sandstone has highest *TVL* which is 12.47 cm and Phyllite have lowest *TVL* value which is 10.22 cm, which suggest Phyllite sample contain best shielding properties among our five sample and Sandstone contain least photon shielding properties and represented as Phyllite < Quartz-I < Granite < Quartz-II < Sandstone.

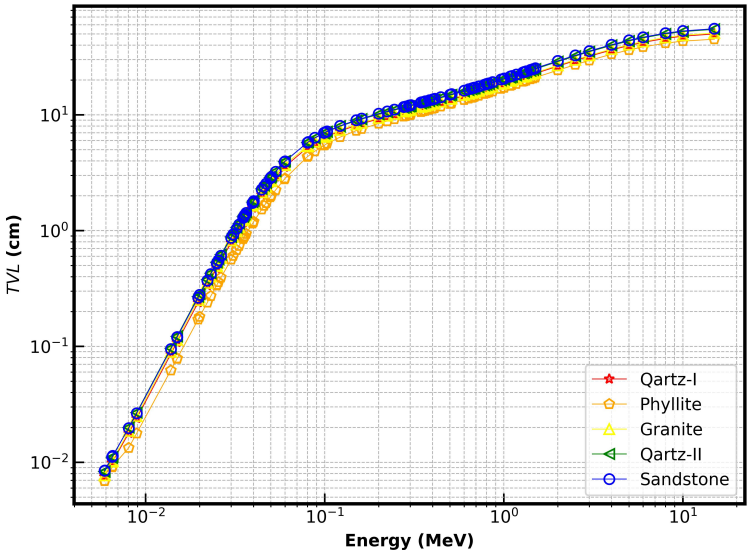

Figure 4.3: Photon energy versus *TVL* of the five rock sample.

Mean free path

Mean free path (*MFP*) is another relevant factor in determining photon attenuation properties. The obtained data from Phy-X/PSD is plotted in graph as shown in Figure 4.4. The graph depicts that the *MFP* increases linearly with energy. Also many other previous work indicates that for better shielding capacity the *MFP* should be as small as possible. From obtained data we can conclude that Sandstone has highest *MFP* which is 5.42 cm and Phyllite have lowest *MFP* value which is 4.44 cm which suggest Phyllite sample contain best shielding properties among our five sample and sandstone contain least photon shielding properties and represented as Sandstone > Quartz-II > Granite > Quartz-I > Phyllite. *MFP* value is significantly affected by density value so that *MFP* reduces with increasing the density. *MFP* has inverse relation with *LAC* [63].

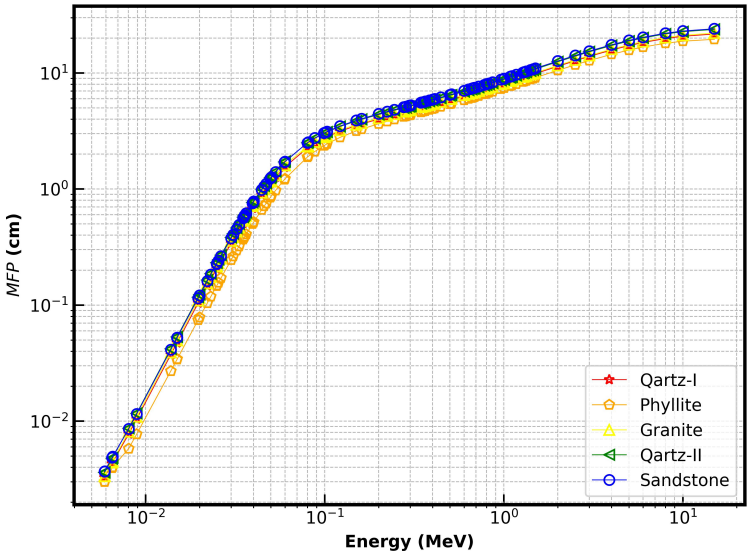

Figure 4.4: Photon energy versus *MFP* of the five rock sample.

Effective atomic number

We have obtained maximum Z_{eff} for phyllite sample which contain maximum Si composition and also contain highest value of weight fraction among selected samples which value is 15.09 shown in Figure 4.5. But in granite sample although Fe content is higher. So granite contain low Z_{eff} value among five sample which value is 14.04. Therefore, from our data we can conclude that phyllite has high Z_{eff} value and also contain best shielding ability and granite rock contain least Z_{eff} value, consequently, has least photon attenuation properties.

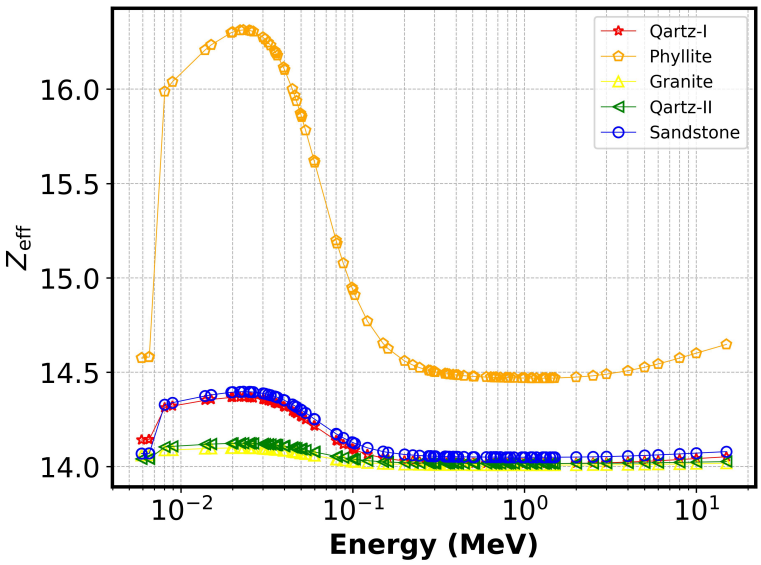

Figure 4.5: Z_{eff} versus photon energy.

Effective electron density

The graphical representation for effective electron density (N_{eff}) is shown in Figure 4.6. Since, effective conductivity and effective electron density are co-related because of properties that they describe about the number of collision of the energetic photons with electrons and converting them to free electrons. Here, both parameter has linear relationship with Z_{eff}. From the obtained data we conclude that Phyllite has highest N_{eff} which value is 2.48×10^{23} electron g^{-1} and Quartz-II has lowest value which is 2.01×10^{23} electron g^{-1} order of shielding capacity is represented as Quartz-II < Granite < Sandstone < Quartz-I < Phyllite.

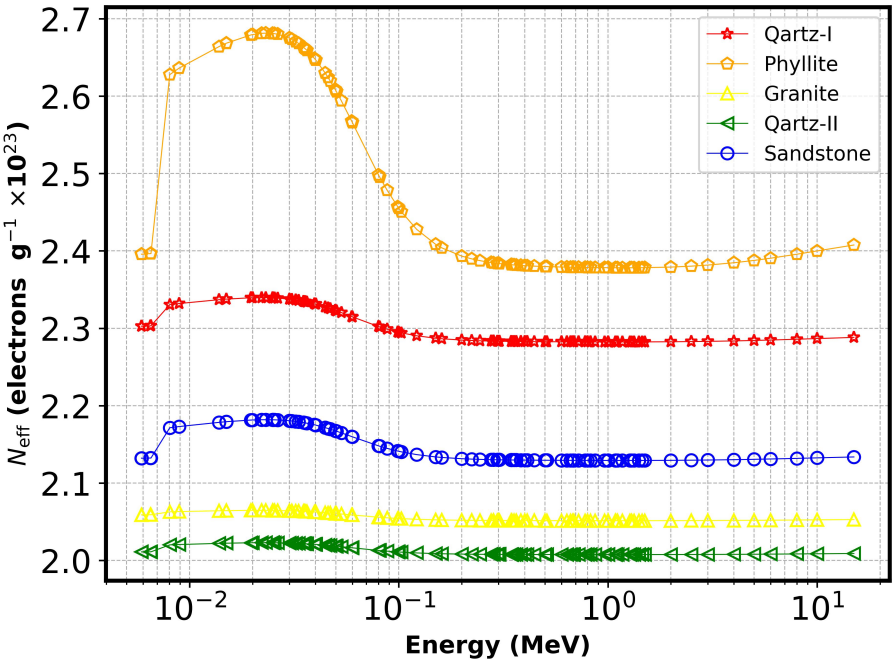

Figure 4.6: N_{eff} versus photon energy.

Effective conductivity

The diagram illustrating efficient conductivity (C_{eff}) is shown in Figure 4.7. Since the characteristics of effective conductivity and effective electron density relate to the quantity of energetic photons that collide with electrons and transform them into free electrons, they are connected. N_{eff} and C_{eff} both contain highest value at low energy and later decreases upto 1.5 MeV and increases slowly upto 15 MeV. Similar pattern of graph is obtained as Z_{eff}. The unit of C_{eff} is siemens per meter (S m^{-1}).

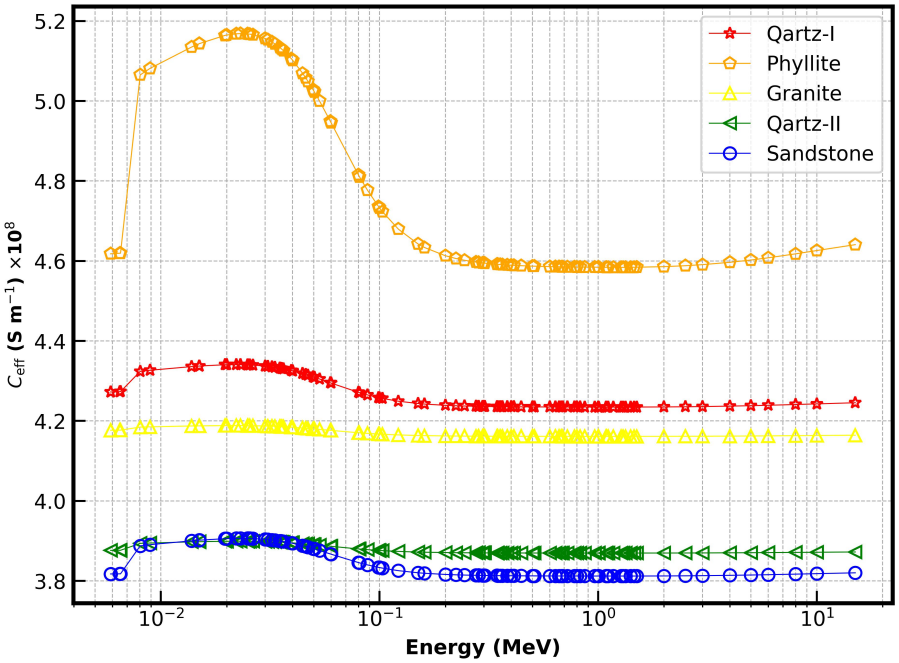

Figure 4.7: C_{eff} versus photon energy.

Fast neutron removal cross-section

The value for fast neutron removal cross-Section (*FNRCS*) is listed in Table 4.2. Among our five selected sample named as Quartz-I, Phyllite, Granite, Quartz-II and Sandstone the high *FNRCS* value is found for Phyllite 0.06 cm^{-1} and low for Sandstone 0.05 cm^{-1}. The increasing order of *FNRCS* value is given as for Sandstone < Quartz-II < Granite < Quartz-I < Phyllite respectively.

Table 4.2: Fast neutron removal cross-section.

Sample	Quartz-I	Phyllite	Granite	Quartz-II	Sandstone
FNRCS (cm^{-1})	5.76 ×10^{-2}	6.14 ×10^{-2}	5.66 ×10^{-2}	5.26 ×10^{-2}	5.18 ×10^{-2}

The graphical representation for fast neutron removal cross-section is shown in Figure 4.8.

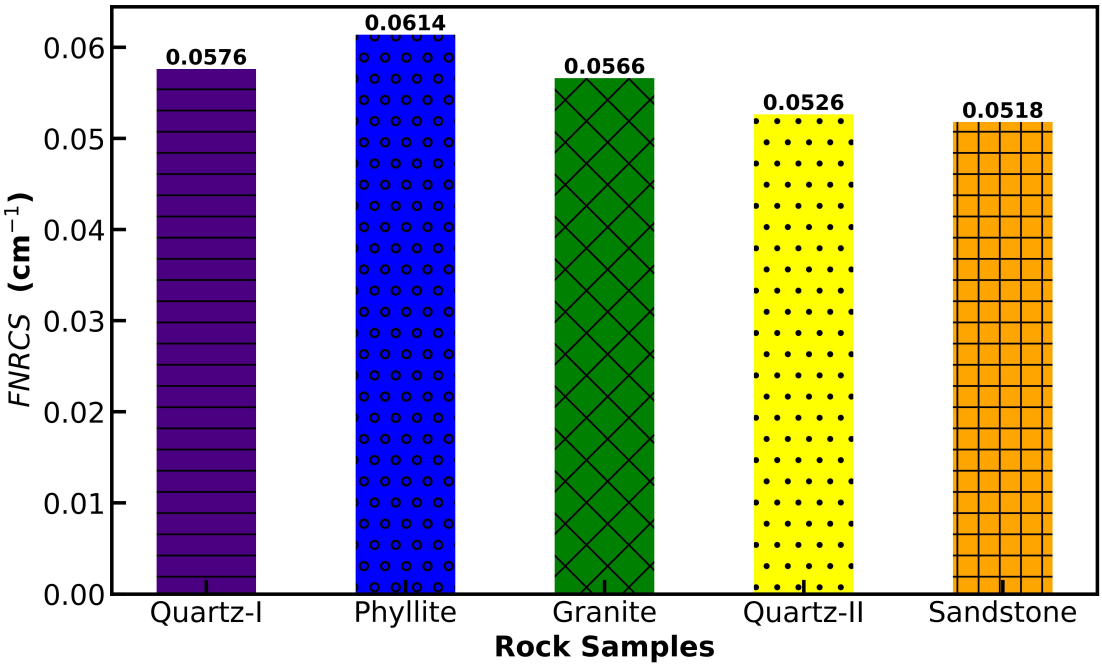

Figure 4.8: Bar diagram for photon energy versus *FNRCS*.

4.3 Linear attenuation coefficient and gamma energy

Tests of the material's shielding ability reveal that photoelectric effects predominate up to ^{241}Am source photon. Table 4.3 displays the data that has been analyzed.

Table 4.3: Representation of the linear attenuation coefficient and associated gamma energy from radionuclei ^{241}Am, ^{152}Eu, ^{137}Cs and ^{60}Co.

Energy	Nuclide	$LAC \times 10^{-2}$ (cm^{-1})				
(MeV)	Symbol	Quartz-I	Phyllite	Granite	Quartz-II	Sandstone
1.38×10^{-2}	^{241}Am	23.59	798.49	38.37	118.60	41.02
2.63×10^{-2}	^{241}Am	3.75	129.94	6.12	19.21	6.53
4.59×10^{-2}	^{152}Eu	0.84	28.58	1.36	4.18	1.47
1.22×10^{-1}	^{152}Eu	0.16	4.65	0.25	0.65	0.29
2.84×10^{-1}	^{137}Cs	0.10	2.63	0.15	0.36	0.18
3.44×10^{-1}	^{152}Eu	0.09	2.40	0.14	0.33	0.17
6.62×10^{-1}	^{137}Cs	0.07	1.79	0.10	0.24	0.12
8.26×10^{-1}	^{60}Co	0.06	1.61	0.09	0.22	0.11
1.17	^{60}Co	0.05	1.35	0.08	0.18	0.09
1.33	^{60}Co	0.05	1.27	0.07	0.17	0.09
2.51	^{60}Co	0.04	0.93	0.05	0.13	0.06

The *LAC* values of the five selected samples are shown in Figure 4.9. These values all correspond to the energy peak of common radio-nuclei, such as Americium ^{241}Am,

Europium ^{152}Eu, Cesium ^{137}Cs, and Cobalt ^{60}Co, that are useful in medical facilities, industrial radiography, and many research facilities for various purposes.

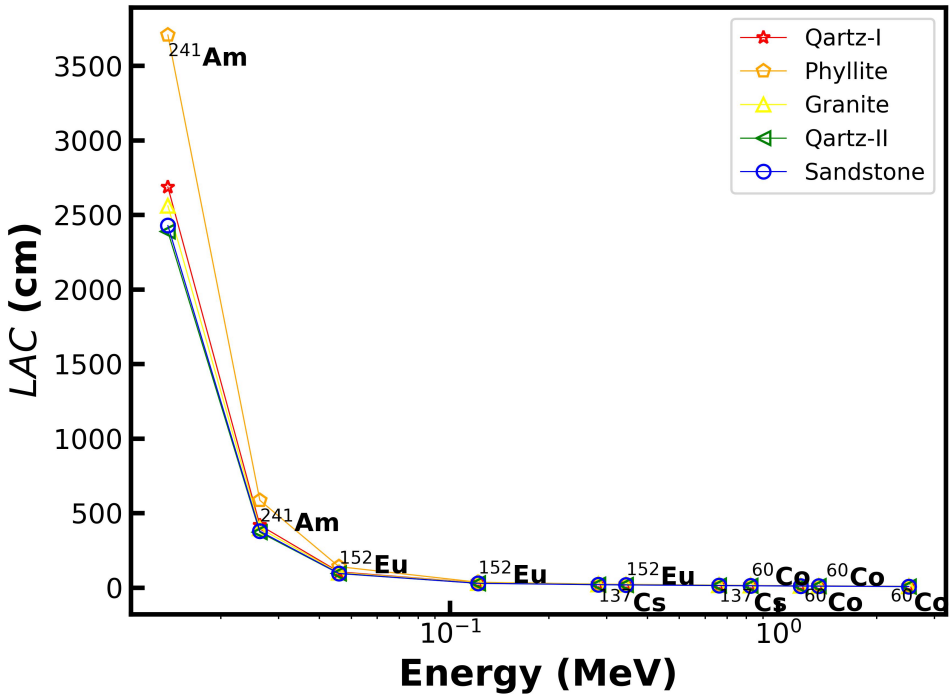

Figure 4.9: Photon energy versus linear attenuation coefficients of gamma ray photons in analysed radionuclei such as ^{241}Am, ^{152}Eu, ^{137}Cs and ^{60}Co.

4.4 Mean free path and associate gamma energy

The mean free path (*MFP*) values of the five selected samples are shown in Figure 4.10. All of these values correspond to the energy peak of common radionuclei, such as Americium ^{241}Am, Europium ^{152}Eu, Cesium ^{137}Cs, and Cobalt ^{60}Co, that are useful in medical facilities, industrial radiography, and many research facilities for various purposes. When the shielding properties of the material are examined, photoelectric effects become dominant up to ^{241}Am source photon. Table 4.4 displays the data analysis.

Table 4.4: Representation of the mean free path and associated gamma energy from radionuclei ^{241}Am, ^{152}Eu, ^{137}Cs and ^{60}Co.

Energy	Nuclide	$MFP \times 10^2$ (cm)				
(MeV)	Symbol	Quartz-I	Phyllite	Granite	Quartz-II	Sandstone
1.38×10^{-2}	^{241}Am	0.04	0.01	0.02	0.01	0.02
2.63×10^{-2}	^{241}Am	0.27	0.01	0.16	0.05	0.15
4.59×10^{-2}	^{152}Eu	1.19	0.04	0.74	0.22	0.68
1.22×10^{-1}	^{152}Eu	6.12	0.22	4.02	1.55	3.41
2.84×10^{-1}	^{137}Cs	10.07	0.38	6.76	2.80	5.57
3.44×10^{-1}	^{152}Eu	10.97	0.42	7.37	3.07	6.07
6.62×10^{-1}	^{137}Cs	14.65	0.56	9.86	4.13	8.10
8.26×10^{-1}	^{60}Co	16.26	0.62	10.94	4.59	8.99
1.17	^{60}Co	19.32	0.74	13.01	5.46	10.68
1.33	^{60}Co	20.62	0.75	13.88	5.82	11.40
2.51	^{60}Co	28.13	1.07	18.92	7.90	15.56

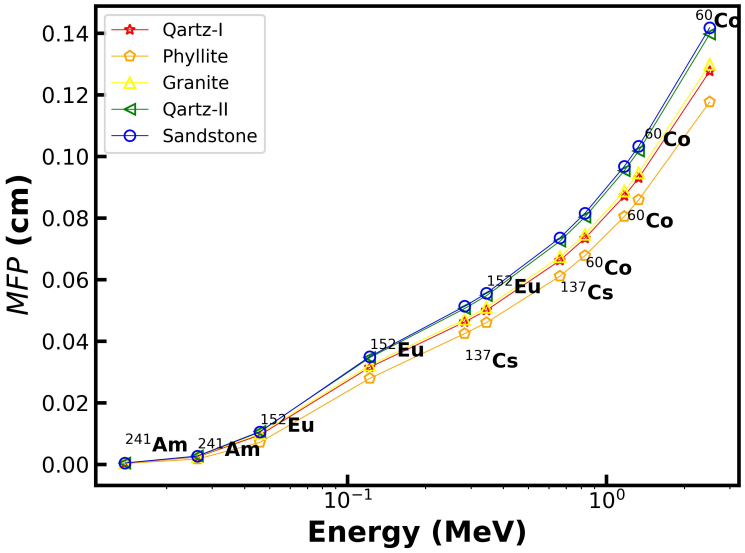

Figure 4.10: Photon energy versus mean free path of gamma ray photons in analysed radionuclei such as ^{241}Am, ^{152}Eu, ^{137}Cs and ^{60}Co.

4.5 Tenth value layer and associated gamma energy

The tenth value layer (*TVL*) of the five selected samples are shown in Figure 4.11. These values all correspond to the energy peak of common radio-nuclei, such as Americium ^{241}Am, Europium ^{152}Eu, Cesium ^{137}Cs, and Cobalt ^{60}Co, that are useful in medical facilities, industrial radiography, and many research facilities for various purposes. When the shielding properties of the material are examined, photoelectric effects become dominant up to source photon. Table 4.5 displays the data analysis.

Table 4.5: Representation of the tenth value layer and associated gamma energy from radionuclei ^{241}Am, ^{152}Eu, ^{137}Cs and ^{60}Co.

Energy	Nuclide	$TVL \times 10^2$ (cm^{-1})				
(MeV)	Symbol	Quartz-I	Phyllite	Granite	Quartz-II	Sandstone
1.38×10^{-2}	^{241}Am	0.10	0.01	0.06	0.02	0.05
2.63×10^{-2}	^{241}Am	0.61	0.02	0.37	0.12	0.35
4.59×10^{-2}	^{152}Eu	2.73	0.08	1.69	0.55	1.56
1.22×10^{-1}	^{152}Eu	14.08	0.49	9.25	3.56	7.86
2.84×10^{-1}	^{137}Cs	23.18	0.88	15.55	6.43	12.83
3.44×10^{-1}	^{152}Eu	25.26	0.96	16.97	7.06	13.98
6.62×10^{-1}	^{137}Cs	33.73	1.29	22.71	9.50	18.65
8.26×10^{-1}	^{60}Co	37.43	1.43	25.20	10.55	20.70
1.17	^{60}Co	44.49	1.70	29.96	12.56	24.60
1.33	^{60}Co	47.47	1.82	31.97	13.40	26.25
2.51	^{60}Co	64.76	2.47	43.56	18.19	35.83

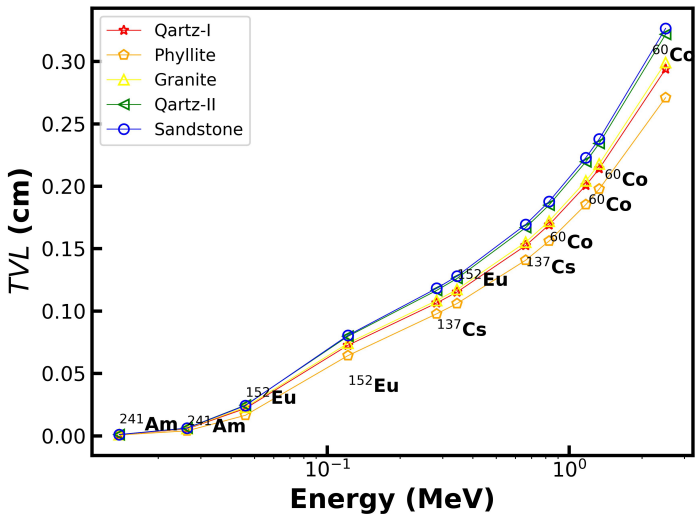

Figure 4.11: Photon energy versus tenth value layer of gamma ray photons in analysed radionuclei such as ^{241}Am, ^{152}Eu, ^{137}Cs and ^{60}Co.

4.5.1 Photon trajectory in rock sample

Geometry for projection of photons from ^{137}Cs source which consists air (Nitrogen 80% and Oxygen 20%) inside the region and outer part is Phyllite rock sample with density 2.67 g cm^{-3} is shown in Figure 4.12. We checked the trajectories of 1 million photons up to 60 ns inside the maze containing air bounded by selected Phyllite rock sample using PHITS code. Figure 4.12(a) represents the trajectory of photons. Figure 4.12(b) represents the trajectory of photons for 1 ns. Figure 4.12(c) represents the trajectory of photons for 6 ns. Figure 4.12(d) represents the trajectory of photons for 18 ns. Fig-

ure 4.12(e) represents the trajectory of photons for 30 ns. Figure 4.12(f) represents the trajectory of photons for 39 ns.

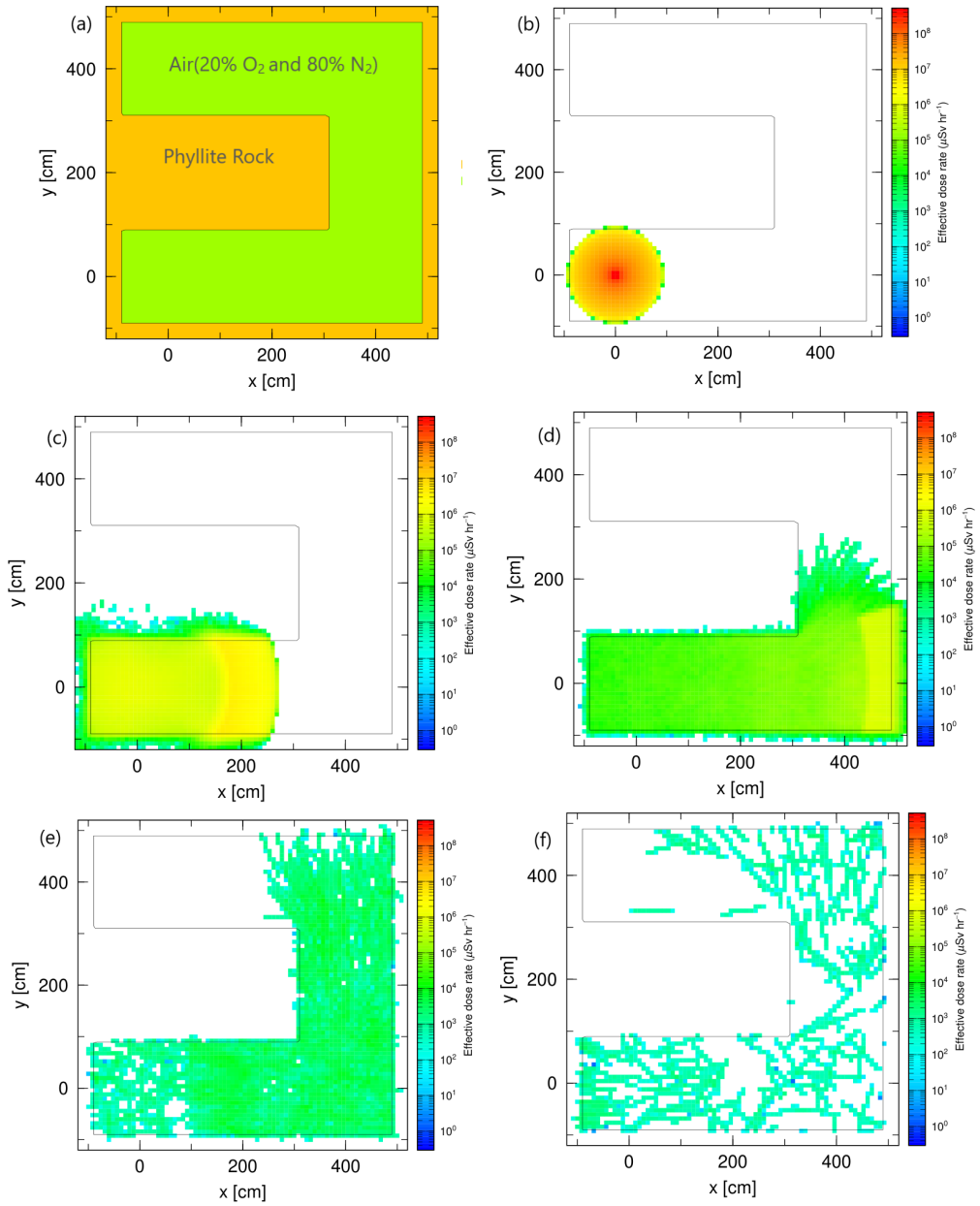

Figure 4.12: (a) Trajectory of 1×10^6 photons originating from 0.662 MeV ^{137}Cs travelling inside the Phyllite rock sample. (b) 1 ns (c) 6 ns (d) 18 ns (e) 30 ns (f) 39 ns .

4.5.2 Comparison with past work and discussion

After comparing the present work at energy range 15 keV to 15 MeV with past work done by Bantan et al.(2020) [35] results are in good agreement and comparable. After decimal nearly coinciding value of the parameter observed.

Table 4.6: Comparison of linear attenuation coefficient (*LAC*) value with published work.

Energy	Linear attenuation coefficient (*LAC*) (cm^{-1})					Reference [35]
(MeV)	Quartz-I	Phyllite	Granite	Quartz-II	Sandstone	Basalt-1
0.662	15.11×10^{-2}	16.37×10^{-2}	14.84×10^{-2}	13.80×10^{-2}	13.60×10^{-2}	24.20×10^{-2}
1.172	11.48×10^{-2}	12.43×10^{-2}	11.28×10^{-2}	10.49×10^{-2}	10.33×10^{-2}	18.99×10^{-2}
1.332	10.76×10^{-2}	11.65×10^{-2}	10.57×10^{-2}	9.83×10^{-2}	9.68×10^{-2}	16.35×10^{-2}
Density ($g\ cm^{-3}$)	2.58	2.67	2.81	2.67	2.48	2.93

mass attenuation coefficient(MAC), linear attenuation coefficient (LAC), half value layer (HVL), tenth value layer(TVL), effective atomic number (Zeff), mean free path (MFP)

Chapter 5

Conclusions and future works

5.1 Conclusions

The concept of radiation shielding is very crucial thing for human safety so shielding is point that protect people from the harmful effects of radiation on their health. This work represents the radiation shielding properties of few selected rock samples from the different region named as Quartz-I, Phyllite, Granite, Quartz-II and Sandstone. To study the radiation shielding we proceeds by physical and chemical analysis using Archimedes's principal and Inductively Coupled Plasma Optical Emission Spectroscopy. After getting density parameter and chemical properties the radiation shielding parameters of our selected rocks sample has been studied using online based Photon Shielding and Dosimetry software (Phy-X/PSD) in energy range from 15 keV to 15 MeV which is very applicable for industrial radiography, radiation therapy, Sterilization of the hospital equipment as well as agriculture and preservation of food. Those type of radiation γ-ray are very important and we focused on shielding nature of natural rocks and measure the various parameters such as linear attenuation coefficient (*LAC*), mass attenuation coefficient (*MAC*), half value layer (*HVL*), tenth value layer (*TVL*), mean free path (*MFP*), fast neutron removal cross-section (*FNRCS*), effective atomic number (Z_{eff}), efficient conductivity (C_{eff}) etc. Also the *MAC* value and *LAC* value obtained by Phy-X/PSD is plotted in graph and found a similar pattern of graph of mass attenuation coefficient and linear attenuation coefficient. Both *MAC* and *LAC* values are found maximum at low energy range (15 keV) and minimum at high energy range (15 MeV). The high value of *MAC* obtained for Phyllite is 6.54 $\text{cm}^2\ \text{g}^{-1}$ which means Phyllite has highest shield-

ing capacity and low *MAC* value for Quartz-II is 5.08 cm^2 g^{-1} this means Quartz-II has lowest shielding capacity in comparision to other four sample. According to obtained value of our five sample Phyllite has highest *LAC* value (17.46 cm^{-1}) and Sandstone has lowest value (13.42 cm^{-1}). According to *LAC* value shielding capacity of five sample increases in following order as Sandstone < Quartz-II < Granite < Quartz-I < Phyllite. Thus Phyllite has best shielding ability among five sample. From the result we find that low *HVL*, *TVL* and *MFP* value obtained for Phyllite rock has the best shielding properties. For our selected samples the Sandstone has high value obtained for *HVL* and *TVL* are 3.75 cm and 12.47 cm respectively and low for Phyllite are 3.08 cm and 10.22 cm respectively. This means Phyllite has highest shielding capacity. Sandstone has highest *MFP* and Phyllite have lowest *MFP* value, which suggest Phyllite sample contain best shielding properties.

By analyzing all data of effective atomic number for five sample and graph we conclude that sample phyllite is best shielding rock among five samples and Sandstone has least radiation shielding ability. For *FNRCS* we found the high value for Phyllite is 0.06 cm^{-1} and low for Sandstone is 0.05 cm^{-1}. The increasing order of *FNRCS* value is given as Sandstone < Quartz-II < Granite < Quartz-I < Phyllite respectively. By analyzing all data and graph we conclude that sample Phyllite is best shielding rock among five samples and Sandstone has least radiation shielding ability. According to shielding ability samples are arranged in increasing order as Sandstone < Quartz-I < Granite < Quartz-II < Phyllite.

5.2 Future work

In future we can diversify our work as:

- More rock samples can be collected from various location throughout country and its radiation shielding can be calculated. As a result, whole country will be benefited by knowing about radiation shielding properties of rock in Nepal.
- More research and study should be conducted on various types of material such as rock, marble, tile, brick etc. These material can also be used for radiation shielding.
- We can develop and manufacture best shielding material which can block heavy ion charged particle. It can be best applicable for space travel and protect astronaut from harmful radiation.
- We can also focus on enhancing shielding capacity of already produced material by doping with high atomic element, different oxides concentration and ions.
- The radioactivity and radiation risk can be calculated further in rock, medicinal plant, water sediment, building material, mining area etc.

References

[1] S. M. Friedman, Bull. At. Sci. **67**, 55 (2011).

[2] S. S. Wong, *Introductory Nuclear Physics* (John Wiley & Sons, 2008).

[3] B. Mavi and I. Akkurt, Radiat. Phys. and Chem. **79**, 933 (2010).

[4] V. F. Weisskopf, Rev. Mod. Phys. **29**, 174 (1957).

[5] S. Patel, *Nuclear Physics: An Introduction* (Wiley, 1991).

[6] Australian Radiation Protection and Nuclear Safety Agency, "Gamma radiation," (2024), accessed: 2024-08-09.

[7] A. Brunetti and S. Buonomo, Radiat. Phys. Chem. **71**, 229 (2004).

[8] L. Harrison and R. Davis, Int. J. Radiat. Phys. **21**, 123 (1996).

[9] G. Bauer, K. Behrens, and P. Schiller, J. Appl. Radiat. Isot. **63**, 217 (2005).

[10] G. F. Knoll, *Radiation Detection and Measurement*, 4th ed. (Wiley, 2010).

[11] E. B. Podgorsak, Med. Phys. **33**, 4772 (2006).

[12] N. Jelley, *Fundamentals of Nuclear Physics* (Cambridge University Press, 1990).

[13] R. J. Glauber, Phys. Rev. **131**, 2766 (1963).

[14] H. D. Young, R. A. Freedman, T. Sandin, and A. L. Ford, *University Physics*, Vol. 9 (Addison-Wesley Reading, MA, 1996).

[15] NASA, "Sources of Ionizing Radiation in Interplanetary Space," (2010), accessed: 2024-08-09.

[16] E. Fermi, Phys. Rev. C: Nucl. Phys. **75**, 1169 (1949).

[17] J. Olomo, M. Akinloye, and F. Balogun, Nucl. Instrum. Methods Phys. Res., Sect. A **353**, 553 (1994).

[18] R. G. Allen, J. Hydrol. Eng. **2**, 56 (1997).

[19] H. Delincée, Trends in Food Science & Technology **9**, 73 (1998).

[20] I. P. Pavlicek, "Safety and Security of Radioactive Sources in Radiography," (2013), accessed: 2024-09-16.

[21] H. Motz and R. Carter, J. Geophys. Res. **68**, 657 (1963).

[22] J. M. Selby, Radiat. Prot. Dosim. **157**, 121 (2013).

[23] D. J. Nagel, Health Phys. **101**, 571 (2011).

[24] R. Prăvălie, AMBIO **43**, 729 (2014).

[25] M. Iqbal, *An Introduction to Solar Radiation* (Elsevier, 2012).

[26] K. S. Krane, *Introductory Nuclear Physics* (John Wiley & Sons, 1991).

[27] J. W. Gofman, *Radiation and Human Health* (Sierra Club Books, San Francisco, CA, 1981).

[28] EPA, "Protecting Yourself from Radiation ," `https://www.epa.gov/radiation/protecting-yourself-radiation` (2020).

[29] F. H. Attix, *Introduction to Radiological Physics and Radiation Dosimetry* (John Wiley & Sons, 2008).

[30] D. Chaney and J. Harris, Phys. Rep. **489**, 149 (2009).

[31] S. Kahn and M. E. Jones, Rev. Mod. Phys. **93**, 025003 (2021).

[32] H. Ebendorff-Heidepriem and D. Ehrt, Radiat. Phys. Chem. **19**, 351 (2002).

[33] J. Smith and J. Doe, J. Radiat. Saf. **15**, 123 (2020).

[34] E. A. Blakely, Health Phys. **79**, 495 (2000).

[35] R. A. Bantan, M. Sayyed, K. Mahmoud, and Y. Al-Hadeethi, Prog. Nucl. Energy **126**, 103405 (2020).

[36] S. S. Obaid, D. K. Gaikwad, and P. P. Pawar, Radiat. Phys. Chem. **144**, 356 (2018).

[37] S. S. Obaid, M. Sayyed, D. Gaikwad, and P. P. Pawar, Radiat. Phys. Chem. **148**, 86 (2018).

[38] I. Akkurt, R. Altindag, T. Onargan, C. Basyigit, S. Kılıncarslan, M. Kun, B. Mavi, and A. Güney, Constr. Build. Mater. **21**, 2078 (2007).

[39] E. Kavaz, H. Tekin, N. Y. Yorgun, Ö. Özdemir, and M. Sayyed, Radiat. Phys. Chem. **162**, 187 (2019).

[40] S. Issa, M. Sayyed, and M. Kurudirek, J. Phys. Sci. **27**, 97 (2016).

[41] M. Durante and F. A. Cucinotta, Rev. Mod. Phys. **83**, 1245 (2011).

[42] S. Islam, K. Mahmoud, M. Sayyed, B. Alim, M. M. Rahman, and A. Mollah, Radiat. Phys. Chem. **172**, 108559 (2020).

[43] Y. Al-Hadeethi, M. Sayyed, and M. Nune, Ceram. Int. **47**, 3988 (2021).

[44] G. Kilic, E. Ilik, K. Mahmoud, R. El-Mallawany, F. El-Agawany, and Y. Rammah, Ceram. Int. **46**, 19318 (2020).

[45] Z. Qian, J. Cai, C. Li, Z. Zhang, and J. Wang, Radiat. Phys. Chem. **185**, 109516 (2021).

[46] M. Sayyed, B. Albarzan, A. H. Almuqrin, A. M. El-Khatib, A. Kumar, D. I. Tishkevich, A. V. Trukhanov, and M. Elsafi, Adv. Mater. **14**, 3772 (2021).

[47] I. Bashter, Ann. Nucl. Energy **24**, 1389 (1997).

[48] D. R. Upadhyay, S. M. Tajudin, and R. Khanal, Ceram. Int. **49**, 23118 (2023).

[49] A. Dulal, D. R. Upadhyay, S. M. Tajudin, and R. Khanal, Materials Research Express **11**, 075202 (2024).

[50] C. Douvris, V. Trey, D. Bussan, G. Bartzas, and R. Thomas, Sci. Total Environ. , 167242 (2023).

[51] E. Şakar, Ö. F. Özpolat, B. Alım, M. Sayyed, and M. Kurudirek, Radiat. Phys. Chem. **166**, 108496 (2020).

[52] T. Sato, Y. Iwamoto, S. Hashimoto, T. Ogawa, T. Furuta, S.-i. Abe, T. Kai, P.-E. Tsai, N. Matsuda, H. Iwase, *et al.*, J. Nucl. Sci. Technol. **55**, 684 (2018).

[53] H. Tekin and O. Kilicoglu, J. Alloys Compd. **815**, 152484 (2020).

[54] A. Levet, E. Kavaz, and Y. N. E. Özdemir, J. Alloys Compd. **819**, 152946 (2020).

[55] M. Halimah, A. Azuraida, M. Ishak, and L. Hasnimulyati, J. Non-Cryst. Solids **512**, 140 (2019).

[56] A. Abouhaswa, M. Al-Buriahi, M. Chalermpon, and Y. Rammah, Appl. Phys. **126**, 1 (2020).

[57] S. Stalin, D. Gaikwad, M. Al-Buriahi, C. Srinivasu, S. A. Ahmed, H. Tekin, and S. Rahman, Ceram. Int. **47**, 5286 (2021).

[58] M. Sayyed, A. Kumar, H. Tekin, R. Kaur, M. Singh, O. Agar, and M. U. Khandaker, Prog. Nucl. Energy **118**, 103118 (2020).

[59] M. Sayyed, Can. J. Phys. **94**, 1133 (2016).

[60] C. Hall and A. Hamilton, Mater. Struct. **49**, 3969 (2016).

[61] W. McKinney, J. Data Sci. **14**, 123 (2017).

[62] Esri, "Arcgis 10.4.1: Advancements in gis technology," =https://www.esri.com/en-us/arcgis/products/arcgis-desktop/overview (2019).

[63] N. J. AbuAlRoos, N. A. B. Amin, and R. Zainon, Radiat. Phys. Chem. **165**, 108439 (2019).

Appendices

Calibration curves

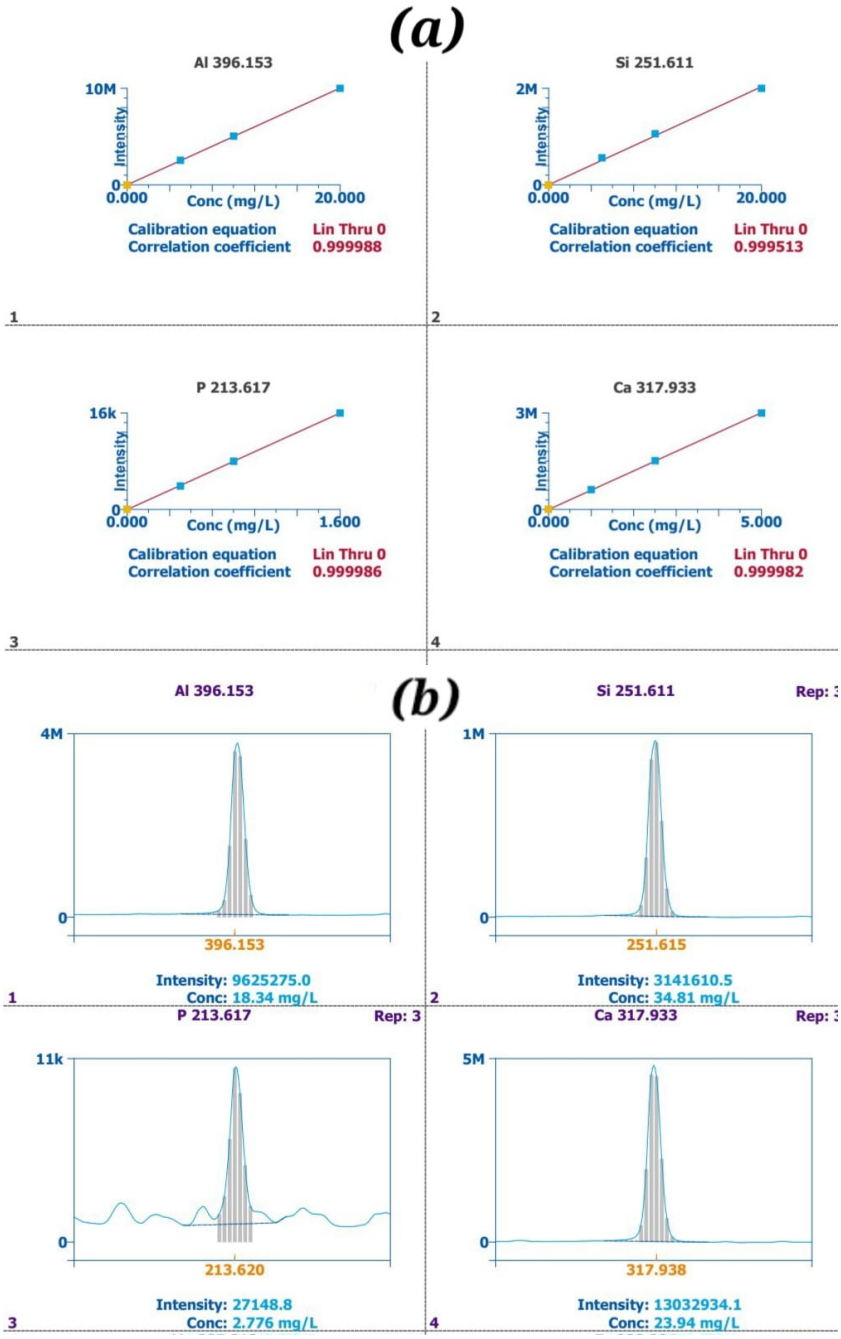

Figure 5.1: (a) Calibration curve without sample (b) Curve with sample

Some photos during experimentions

(a) **(b)**

Figure 5.2: (a) Making plate sheet of rocks. (b) Sample preparation.

(a) **(b)**

Figure 5.3: (a) Powder form rock sample. (b) Measuring the gamma ray shielding.

(a)

(b)

Figure 5.4: (a) Well prepared sample for ICP-OES. (b) Storing the prepared sample.

(a)

(b)

Figure 5.5: (a) Prepared sample to test. (b) Sample testing in laboratory.

(a)

(b)

Figure 5.6: (a) Evaluating density of rocks sample. (b) Measuring the thickness of sample.